Age-Related Differences in Human Cortical Microstructure Depend on the Distance to the Nearest Vein

†Christoph Knoll[1,2], †Juliane Doehler[1,2], Alicia Northall[1,2], Stefanie Schreiber[2,4,5], Johanna Rotta[5,8], Hendrik Mattern[2,3,4], *Esther Kuehn[6,7,1]

[1] Institute of Cognitive Neurology and Dementia Research (IKND), Otto-von-Guericke-University Magdeburg, Magdeburg, Germany
[2] German Center for Neurodegenerative Diseases (DZNE), Magdeburg, Germany
[3] Department Biomedical Magnetic Resonance (BMMR), Otto-von-Guericke-University Magdeburg, Magdeburg, Germany
[4] Center for Behavioral Brain Sciences (CBBS), Magdeburg, Germany
[5] Department of Neurology, Otto-von-Guericke University Magdeburg, Magdeburg, Germany
[6] Hertie Institute for Clinical Brain Research (HIH), Tübingen, Germany
[7] German Center for Neurodegenerative Diseases (DZNE), Tübingen, Germany
[8] Department of Neurology, Katharinenhospital, Klinikum Stuttgart, Stuttgart, Germany

*** Correspondence**
Esther Kuehn
esther.kuehn@uni-tuebingen.de

† these authors contributed equally to this work and share first authorship

Abstract

Age-related differences in cortical microstructure are used to understand the neuronal mechanisms that underlie human brain ageing. The cerebral vasculature contributes to cortical ageing, but its precise influence on age-related differences in cortical microstructure is poorly understood. In a cross-sectional study, we combine venous imaging with vessel distance mapping (VDM) to investigate the influence of venous distances on age-related differences in the microstructural architecture of the cortex. We focus on primary somatosensory cortex (S1) and primary motor cortex (M1) as both show age-related alterations linked to neurodegeneration and behavioural decline. We scanned 18 younger adults and 17 older adults at a 7T MRI scanner to measure age-related changes in quantitative T1 (qT1) values and positive QSM (pQSM) values at 0.5 mm isotropic resolution as proxies for cortical myelin and cortical iron content, respectively. We modelled different cortical depths using an equi-volume approach and assessed the distance of each voxel in each layer to its nearest vein using VDM. Our data reveal a dependence both of cortical qT1 and cortical pQSM values on venous distance. In addition, there is an interaction between venous distance and age on qT1 values, driven by lower myelination in older compared to younger adults in voxels that are farther away from a vein and higher myelination in older adults in voxels that are closer to a vein. This effect is particularly pronounced in M1 and indicates that the venous distance may act as a protective mechanism in healthy ageing. Together, our data show that the local venous architecture explains a significant amount of variance in standard measures of cortical microstructure, and should be considered in neurobiological models of human brain organisation and cortical ageing.

Keywords: laminar imaging, ultra-high field MRI, iron, vasculature, arteries, neurodegeneration

1. Introduction

Age-related differences in cortical microstructure are used to understand the neuronal mechanisms that underlie human brain ageing and neurodegeneration. Vascular supply patterns in the brain vary between individuals (Bernier et al., 2018; Huck et al., 2019), influence cortical microstructure and functional decline (Perosa et al., 2020; Vockert et al., 2021), and explain brain pathology (Schreiber et al. 2023). However, the contribution of the local vascular architecture on age-related changes in cortical microstructure is poorly understood. This knowledge gap prevents us from understanding the mechanisms that underlie human cortical ageing and potential protective factors.

The human cortex is permeated by a dense net of blood vessels that is highly variable in location and diameter (Huck et al., 2019). Vascular changes are a risk factor for all-cause dementia (Ungvari et al. 2021), and antihypertensive treatment can lower dementia incidence (Peters et al. 2022). A human MRI study reported that participants with cerebral small vessel disease who show a double-supply pattern of hippocampal vascularization perform better in cognitive tests compared to those with a single-supply pattern (Perosa et al., 2020). Vascular health is regarded as a key driver for resilience in ageing, for example by maintaining blood flow and neuronal metabolism (Arenaza-Urquijo et al. 2019).

However, it is still unclear how individual vascular supply patterns interact with age-related cortical degeneration. More specifically, cortical locations that are more distant to the next larger blood vessel might be more prone to age-related structural alterations, such as myelin loss (Cho et al. 1997; Callaghan et al. 2014; Grydeland et al. 2019) and iron accumulation (Callaghan et al. 2014; Acosta-Cabronero et al. 2016; Betts et al. 2016; Northall et al. 2023a), in case ageing blood vessels particularly reduce supply to locations that are farther away from major branches (Hypothesis 1, H1). Alternatively, myelin loss and iron accumulation might be more pronounced at cortical locations that are closer to blood vessels, because age-related substance accumulation occurs near blood vessels (Farkas et al. 2006) (Hypothesis 2, H2). Finally, one could hypothesise that cortical degeneration occurs independent of the distance to the next blood vessel (Hypothesis 3, H3).

To test these three hypotheses, we compared two extreme age groups (healthy younger adults < 30 years of age, healthy older adults > 65 years of age) using ultra-high resolution magnetic

resonance imaging at 7 Tesla (7T MRI). Quantitative T1 values (qT1) were used as validated proxy for cortical myelin content (Dinse et al., 2015; Stüber et al., 2014; Haast et al. 2016), and quantitative susceptibility mapping (QSM) was used to quantify cortical iron (Langkammer et al., 2012; Deistung et al. 2013; Hametner et al. 2018; Acosta-Cabronero et al. 2016; Betts et al. 2016). We focus on primary somatosensory cortex (S1) and primary motor cortex (M1) as both areas play an important role in ageing and neurodegeneration, and venous density in S1 and M1 has been associated with myelin loss and decline of sensorimotor function in older adults (Schreiber et al. 2023). Ultra-high resolution QSM images were used for vein identification, and Vessel Distance Mapping (VDM) for linking age-related changes in layer-specific cortical microstructure to the distance to the nearest vein (Mattern et al. 2021a; Garcia-Garcia et al. 2023).

Together, we combine MRI proxies of cortical myelin and iron with VDM to test whether age-related changes in S1 and M1 microstructure depend on the distance to the nearest vein. This work contributes to our understanding of how the individual vascular architecture relates to microstructural variance in the ageing cortex, and provides critical insights into the mechanisms of cortical ageing.

2. Materials & Methods

2.1. Participants

35 healthy volunteers (n=18 younger adults: M=25 years, SD=3 years, ranging from 21 to 29 years, 9 females; n=17 older adults: M=70 years, SD=4 years, ranging from 65 to 77 years, 10 females) were recruited from the database of the German Center for Neurodegenerative Diseases (DZNE), Magdeburg, Germany and participated in our cross-sectional study. All participants were right-handed (laterality index ranging from +40 to +100; Oldfield, 1971).

Ultra-high field MRI contraindications (e.g. presence of active implants, non-removable metallic objects, tinnitus, tattoos/permanent makeup, claustrophobia, pregnancy, consumption of alcohol or drugs), chronic illness, psychiatric or neurological disorders, central acting medications and impaired hand function were exclusion criteria. 1/17 older adults underwent carpal tunnel surgery on both hands. However, no complaints were reported and no outliers were detected in sensorimotor tasks (see **Supplementary Table 1**).

With respect to vascular health, 6/17 older adults reported a history of hypertension that was

well-controlled with specific medication in all cases (see **Table 1**). Two experienced neurologists evaluated vascular health of older adults according to the STandards for ReportIng Vascular changes on nEuroimaging (STRIVE-2, Wardlaw et al. 2013, Duering et al. 2023) for the detection of cerebral small vessel diseases, and the guideline by Chen et al. (2022) for the detection of thromboses. We detected microbleeds, cortical superficial siderosis, lacunae and/or enlarged perivascular spaces in 6/17 older adults (see **Table 1**). All neurological anomalies were detected outside S1 and M1. In total, 9/17 older adults showed vascular health risk factors (i.e., hypertension and/or signs of cerebral small vessel diseases). Besides, participants showed no medical illnesses. As indicated by the 'Montreal Cognitive Assessment' (MoCA; Nasreddine et al., 2005), there were no signs of cognitive impairments (mean score 28.33 ± 1.45), except for one older adult who had a MoCA score of 21 (MoCA ≥ 26 is considered normal; Nasreddine et al., 2005; see **Table 1**). Because this participant performed equally well in sensorimotor tasks compared with all other older adults (i.e., no extreme outliers, see **Supplementary Table 1**), we kept the data in the analysis. There were no professional musicians among the participants (Elbert et al., 1995; Ragert et al., 2004; Schwenkreis et al., 2007).

All participants were paid for their attendance and provided written informed consent. The study was approved by the local Ethics committee of the Otto-von-Guericke University Magdeburg, Germany. Structural S1 data of younger adults (Doehler et al., 2023) and structural M1 data of younger and older adults (Northall et al., 2023a) were published previously. However, in both studies, the factor of venous architecture was not investigated.

				STRIVE-2 Criteria					
Participant	MoCA	Hypertension	Thrombosis	Cerebral Microbleeds	cSS	Microinfarcts	Lacunae	EPVS	Composite Score
1	26	n	n	n	n	n	n	n	1
2	21	n	n	n	n	n	n	n	1
3	29	y	n	n	n	n	subcortical frontal L (1)	n	2
4	28	n	n	n	n	n	n	n	1
5	28	n	n	temporal R (1)	frontal R	n	frontal L, parietal L+R (3)	n	4
6	29	n	n	n	n	n	n	n	1
7	30	y	n	n	n	n	deep white matter L+R (3)	n	2
8	26	n	n	n	n	n	n	multiple	2
9	27	y	n	n	n	n	n	n	1
10	28	y	n	n	n	n	n	n	1
11	26	n	n	temporal R (1)	n	n	n	n	2
12	26	n	n	n	n	n	n	n	1
13	-	y	n	n	n	n	n	n	1
14	28	n	n	n	n	n	n	n	1
15	29	y	n	occipital R (1)	parietal R, frontal L+R	n	n	multiple	4
16	26	n	n	n	n	n	n	n	1
17	30	n	n	n	n	n	n	n	1

Table 1. MoCA scores and vascular health rating for older adults. The 'Montreal Cognitive Assessment' (MoCA) score is an indicator of cognitive impairment. A MoCA score ≥ 26 is considered normal. Vascular health is given as self-reported history of hypertension (y = yes, n = no), visually detected thrombosis following the guideline by Chen et al. (2022) and the STRIVE-2 criteria (Duering et al. 2023; cSS = cortical superficial siderosis; EPVS = enlarged perivascular spaces). In parentheses, the number of lesions are detailed. The composite score reflects the sum of positive STRIVE-2 criteria (1 = no positive criterion, 2 = one positive criteria, 3 = two positive criteria, 4 = three positive criteria).

2.2. MRI Data Acquisition

All participants took part in one structural 7T-MRI scanning session. The data were acquired at a Siemens MAGNETOM scanner located in Magdeburg, Germany, using a 32-channel head coil. First, MP2RAGE (Marques et al. 2010) whole brain images were acquired at 0.7 mm isotropic

resolution (240 sagittal slices, field-of-view = 224 mm, repetition time = 4800 ms, echo time =2.01 ms, inversion time TI1/TI2 = 900/2750 ms, flip angle = 5 ◦ /3 ◦, bandwidth = 250 Hz/Px, GRAPPA 2). Second, MP2RAGE part-brain images (optimised to target M1 and S1) were acquired at 0.5 mm isotropic resolution (208 transversal slices, field-of-view read = 224 mm, repetition time = 4800 ms, echo time = 2.62 ms, inversion time TI1/TI2 = 900/2750 ms, flip angle = 5 ◦ /3 ◦, bandwidth = 250 Hz/Px, GRAPPA 2, slab oversampling = 7.7%). Finally, part-brain susceptibility-weighted images (optimised to target M1 and S1) were acquired at 0.5 mm isotropic resolution using a 3D GRE sequence (Haacke et al. 2004) (208 transversal slices, field-of-view read = 192 mm, repetition time = 22 ms, echo time = 9.00 ms, flip angle =10◦, bandwidth = 160 Hz/Px, GRAPPA 2, slice oversampling = 7.7%). The total scanning time was around 60 minutes.

2.3. Image Preprocessing

We used the same preprocessing pipeline as described previously (Doehler et al. 2023; Northall et al. 2023). In short, data quality was ensured by two independent raters. QSM images were reconstructed using the Bayesian multi-scale dipole inversion (MSDI) algorithm as implemented in qsmbox (version v2.0, freely available for download: https://gitlab.com/acostaj/QSMbox, Acosta-Cabronero et al., 2018). MP2RAGE and non-normalized QSM data (Betts et al., 2016) were processed using the Java Image Science Toolkit (JIST; Lucas et al., 2010) and CBS Tools (Bazin et al., 2014) as plug-ins for the Medical Image Processing, Analysis, and Visualisation software (MIPAV; https://mipav.cit.nih.gov/).

Slab qT1 images were registered to upsampled whole-brain qT1 images (Advanced Normalization Tools (ANTs) v1.9x, Avants et al., 2011, embedded in CBS-tools) in one single step before slab and whole-brain images were merged. The MP2RAGE Skull Stripping Algorithm (CBS Tools; Bazin et al, 2014) was used to remove extra-cranial tissue, the MP2RAGE Dura Estimation algorithm (CBS Tools; Bazin et al, 2014) to remove dura mater. Dura mater masks were manually checked and eventually refined to ensure that all non-brain tissue was removed. QSM images were registered to the merged whole brain qT1 images using the software ITK-SNAP (version 3.6.0, freely available for download at www.itksnap.org).

Cortical segmentation was calculated on the UNI image, using the Topology-preserving Anatomy-Driven Segmentation (TOADS) algorithm (Bazin & Pham, 2007). To estimate the

boundaries between the white matter (WM) and the grey matter (GM), and between the GM and cerebrospinal fluid (CSF), the CRUISE (Cortical Reconstruction Using Implicit Surface Evolution) algorithm (Han et al, 2004) was used. Resulting level set images (surfaces in Cartesian space using a level set framework; Sethian, 1999) were optimised to precisely match M1 and S1 by thresholding the inner (WM-GM) and outer (CSF-GM) border to a maximum value of -5.0 and -2.0 for M1 and -2.8 and -0.2 for S1, respectively (based on empirical optimization; Northall et al., 2023; Doehler et al., 2023).

The cortex was divided into 21 cortical depths using the validated equi-volume model (Waehnert et al. 2014). After removing the three most superficial and the two deepest cortical depths to reduce partial volume effects (Kuehn et al., 2017; Tardif et al., 2015), the remaining 16 depths were averaged into four equally-spaced cortical depths (SF=superficial, OM=outer-middle, IM=inner-middle, DP=deep) (Kuehn et al. 2017). The estimated cortical depths do not correspond to anatomical layers, because the cortex was divided into equally-spaced compartments based on *in vivo* MRI data. Finally, we sampled the non-merged high-resolution qT1 and QSM slab data (ensuring high data quality) to derive proxies for myelin content (qT1 values) and iron content (positive QSM values, i.e. pQSM).

2.4 Vessel segmentation and Vessel Distance Mapping (VDM)

To extract vessels from the QSMs, we used the Filtered Vessels module (v3.0.4; CBS Tools; Bazin et al., 2014). The vasculature was segmented using a MRF (Markov Random Field) diffusion technique. Previous validation studies revealed that this technique captures venous architectures with high precision (Bazin et al., 2016). The resulting vessel probability map represents the probability of each voxel belonging to a vessel (1=highest probability, 0=lowest probability).

For computing VDMs (Garcia-Garcia et al. 2023), individual vessel probability maps were binarized. For thresholding, we used the openly available sMall vEsseL sEgmenTa-Tion pipelinE (OMELETTE, Mattern, 2021b, https://gitlab.com/hmattern/omelette). Thresholds were set automatically using a 3-class Otsu histogram analysis (returning a lower and upper threshold). Voxels above the upper threshold were considered as vessels, voxels below the lower threshold were considered as background. To classify vessels between the lower and the upper threshold, hysteresis thresholding was used (Fraz et al., 2011), which considers a voxel

belonging to a vessel only if it is connected to a voxel with a value above the upper threshold. A Euclidean distance transformation (Maurer et al., 2003) was applied to the thresholded data to compute the distance to the closest segmented vein per voxel, generating vessel distance maps (VDMs). VDMs were multiplied with binarized cortical depths masks and S1/M1 masks, resulting in one VDM per cortical depth, participant, and brain area (see **Figure 1** for overview).

qT1 images were multiplied with inverted binarized vessel probability masks (extracting values not overlapping with identified veins). Reconstructed QSM images were multiplied with inverted binarized vessel probability masks after thresholding them for positive values (pQSM values). Resulting qT1 and pQSM values were sampled at different cortical depths.

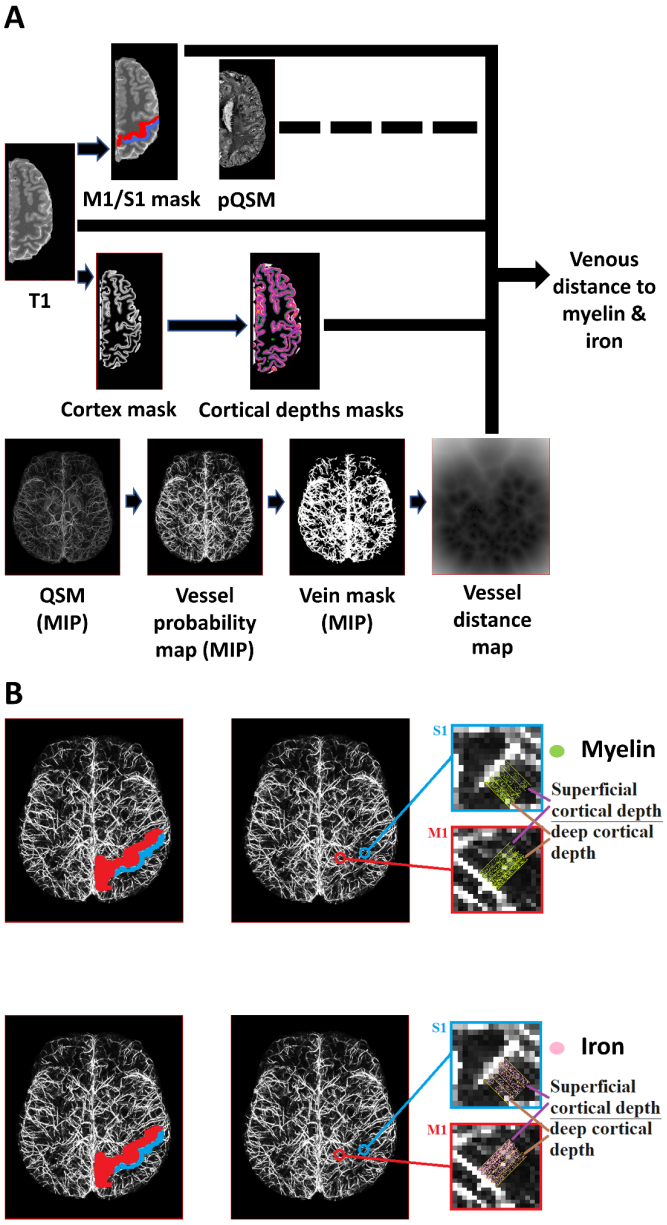

Figure 1: **Overview Methodology and Analysis**. **A:** qT1 and QSM images were sampled at different cortical depths (cortical depths masks) after the cortex segmentation (cortex masks). Masks were applied to extract data from the primary motor cortex (M1, *red mask*) and the primary somatosensory cortex (S1, *blue mask*). Quantitative Susceptibility Maps (QSM; displayed as Maximum Intensity Projections, MIP) were used to extract the vessel probability maps (including intensity values between 0 and 1) to identify venous vasculature. A hysteresis filter was used to generate a binarized vein mask before a Euclidean distance transformation was applied to compute the Vessel Distance Map (VDM). Individual VDMs were multiplied with binarized cortical depths masks and then applied to the qT1 image before resulting parameter maps were multiplied with binarized M1/S1 masks (*analysis pathway shown as black lines*). Please note that the same analysis pathway was applied to the pQSM data (*black dotted line*). **B:** Shown are masks covering left M1 (*red*) and left S1 (*blue*) together with the vessel probability map of one example participant. Magnified images show extracted cortical depth compartments in relation to the distance to the nearest vein.

2.5. Anatomical definition of S1 and M1

M1 and S1 masks were manually generated using an operational definition based on anatomical landmarks extracted from cytoarchitectonic (Geyer et al., 1999), fMRI (Yousry et al., 1997) and multimodal parcellation studies (Glasser et al. 2016, Glasser and Van Essen 2011), following a standardised procedure (for details see Northall et al., 2023a; Northall et al. 2023b; Doehler et al., 2023) using the manual segmentation tool in ITK-SNAP (v3.8.0, Yushkevich et al., 2006). The hand knob served as a localiser to identify the hand area in M1 (97-100% accuracy, Yousry et al., 1997). We masked all axial slices in which the hand knob was visible, and extended the masks inferior and superior to the hand knob until the precentral gyrus was completely covered (e.g. Northall et al., 2023a; Northall et al. 2023b). S1 masks were drawn from the crown of the postcentral gyrus to the fundus of the central sulcus (Doehler et al., 2023), covering area 3b, and parts of area 1 and area 3a (Geyer et al., 1999). Only those slices were masked in which the postcentral gyrus was visible. For M1 masks also include medial M1, whereas S1 masks mainly cover lateral S1. Resulting masks were plotted in reference to co-registered Freesurfer labels to ensure that the delineated regions overlap with those outlined by automated approaches. As normalised anatomical data often falls short in capturing nuanced inter-individual distinctions in high-resolution MRI data due to smoothing effects and/or anatomical landmarks deviating from functional circuit structures (Guntupalli et al., 2016), we chose an individual segmentation approach, where no normalisation is needed and the individual anatomy is considered.

2.6 Distance Binning

Each cortical VDM was discretized into 5 bins, which represent levels of different distances to the nearest vein (i.e., 0.01–2 mm, 2.01–4 mm, 4.01–6 mm, 6.01–8 mm and 8.01–10 mm), for each given voxel in M1 and S1. Binning was used to obtain different distance conditions for statistical group analysis. We chose five bins to include a minimum of 4 voxels per distance condition. Resulting binned data (5 VDMs per cortical depth and brain region) were multiplied with qT1 and pQSM images.

2.7. Vascular Health Evaluation

Two experienced neurologists evaluated vascular health of older adults based on visual inspection of MR scans. Following the guideline by Chen et al. (2022), thromboses were investigated using part-brain QSM data in comparison with part-brain SWI data. According to the STRIVE-2

recommendations, microbleeds and cortical superficial siderosis were investigated based on the part-brain SWI data, whereas lacunae and microinfarcts were examined using whole-brain T1-weighted images (MP2RAGE).

2.8. Behavioural Tasks

Tactile detection thresholds of the right index fingertip were assessed using fine hair stimuli (Semmes-Weinstein monofilaments; Baseline, Fabrication Enterprises Inc., White Plains, NY, USA; stimuli intensities: 0.008 g, 0.02 g, 0.04 g, 0.07 g, 0.16 g, 0.4 g, 0.6 g, 1.0 g, 1.4 g, 2.0 g, see **Supplementary Methods** for details), tactile 2-point discrimination performance of the right index fingertip was assessed using a standard procedure (Kalisch et al., 2008; Kuehn et al., 2017; Pleger et al., 2016, see **Supplementary Methods** for details), and sensorimotor integration performance of the right hand was assessed with a custom made pressure sensor (held between the thumb and index finger of the right hand) (Vieluf et al., 2013, see **Supplementary Methods** for details).

2.9. Statistical Analyses

To investigate the interaction between venous distance and cortical microstructure, we calculated mixed-effects ANOVAs on qT1 and pQSM values with age group (younger, older) as between-subjects factor, and brain area (M1, S1), cortical depth (SF, OM, IM, DP) and distance to the nearest vein (0.01-2 mm, 2.01-4 mm, 4.01-6 mm, 6.01-8 mm, 8.01-10 mm; as well as: 2.01-4 mm, 4.01-6 mm, 6.01-8 mm, 8.01-10 mm) as within-subjects factors. Associated statistical analyses were performed using SPSS (IBM Corp. Released 2012. IBM SPSS Statistics for Windows, Version 21.0. Armonk, NY: IBM Corp.). Sample distributions were tested for normality using Shapiro-Wilk's test in combination with visual inspections (see **Supplementary Figure 1**, **Supplementary Figure 2**). Homogeneity of variances was tested with Levene's test. In case of sphericity violations, Greenhouse-Geisser-corrected results were used. Post-hoc tests were performed as two-tailed paired-samples *t*-tests to follow up within-subjects effects and as two-tailed independent samples *t*-tests to follow up between-subjects effects. Given the bin representing the closest distance to the nearest veins (i.e., 0.01-2 mm) contained no qT1 values in 12/18 younger adults and no pQSM values in 11/18 younger and 5/17 older adults, we report statistical analyses both, for 5 distance conditions with imputed missing values for the closest distance (i.e., 0.01-2mm), using the method of multiple monotone imputation based on linear

regression, and for 4 distance conditions (i.e., excluding the closest distance condition). The significance level was set to p=0.05. In addition to uncorrected p-values, we report Holm-Bonferroni corrected p-values for post-hoc tests (i.e., multiple comparisons). Generalised Eta-squared (η^2_G) was calculated as an effect size estimator for ANOVAs (Lakens, 2013). Cohen's benchmarks of 0.06 and 0.14 for medium and large effects, respectively, were applied (Cohen, 1988).

To control for a possible effect of vascular health risk on qT1 values and a possible interaction effect between vascular health risk and distance to the nearest vein in older adults, we calculated linear regression models (random intercept models), using the lmer function from the lme 4 package (version 1.1.33) in R (version 4.2.2, R Core Team, 2022). We compared two models (model 1: qT1 ~ distance to nearest vein + vascular risk + 1/participant; model 2: qT1 ~ distance to nearest vein + vascular risk + distance to nearest vein:vascular risk + 1/participant) with a null model (qT1 ~ distance to nearest vein + 1/participant) to test the influence of vascular health risk in relation to the distance to the nearest vein. For pQSM values, we performed a simple linear regression (pQSM ~ vascular risk) using the lm function from the stats package (version 4.2.2) in R.

3. Results

3.1. Age-related differences in cortical myelination are driven by the distance to the nearest vein

To test for the effect of venous distance on age-related changes in cortical myelination, we computed an ANOVA with the factors, age (younger, older), brain area (S1, M1), cortical depth (SF, OM, IM, DP) and venous distance (0.01-2 mm, 2.01-4 mm, 4.01-6 mm, 6.01-8 mm, 8.01-10 mm) on qT1 values. As expected, there is a significant main effect of brain area (see **Table 2**) driven by lower qT1 values (higher myelination) in M1 compared to S1 (see **Figure 2B**), and a significant main effect of cortical depth driven by more myelinated deep layers in M1 and S1 (see **Table 2**, **Figure 2C**).

There is also a significant main effect of venous distance (see **Table 2**) driven by significantly higher qT1 values (reduced myelination) at distances 0.01-2 mm compared to distances 2.01-4 mm ($t(34)=4.428$, $p=9.353*10^{-5}$, $p_{Holm\text{-}Bonferroni}=3.74*10^{-4}$), at distances 2.01-4 mm compared to

distances 4.01-6 mm (t(34)=2.710, p=0.010, $p_{Holm\text{-}Bonferroni}$=0.03), and at distances 4.01-6 mm compared to distances 6.01-8 mm (t(34)=2.371, p=0.024, $p_{Holm\text{-}Bonferroni}$=0.048, see **Table 2** for means and standard errors of compared conditions). This shows that, in both younger and older adults, there is greater cortical myelination with greater distance to the nearest vein (see **Figure 2D)**.

The significant interaction between brain area and venous distance on qT1 values (see **Table 2**) reveals that this effect is mainly driven by M1 rather than S1. More specifically, post hoc *t*-tests show that in M1, qT1 values are significantly lower for distances 2.01-4 mm compared to distances 0.01-2 mm (t(34)=4.190, p=$1.871*10^{-5}$,$p_{Holm\text{-}Bonferroni}$=$7.484*10^{-5}$), for distances 4.01-6 mm compared to distances 2.01-4 mm (t(34)=4.443, p=$8.952*10^{-5}$, $p_{Holm\text{-}Bonferroni}$=$2.686*10^{-4}$), and for distances 6.01-8 mm compared to distances 4.01-6 mm (t(34)=2.640, p=0.012, $p_{Holm\text{-}Bonferroni}$=0.024). In S1, in the other hand, qT1 values are only lower for distances 0.01-2 mm compared to distances 2.01-4 mm (t(34)=2.402, p=0.022, $p_{Holm\text{-}Bonferroni}$=0.088), whereas all other comparisons are not significant (2.01-4 mm versus 4.01-6 mm: t(34)=-0.823, p=0.416; 4.01-6 mm versus 6.01-8 mm: t(34)=1.063, p=0.295; 6.01-8 mm versus 8.01-10 mm: t(34)=0.790, p=0.435, see **Figure 2F**).

We then explored potential age effects and detected no significant main effect of age (see **Table 2**, **Figure 2A**) and no significant interaction between age and brain area (see **Table 2**), but a significant interaction between age and venous distance on qT1 values (see **Table 2**). Post hoc *t*-tests reveal significantly lower qT1 values (higher myelination) in older adults at venous distances 0.01-2 mm compared to younger adults (t(23.345)=3.145, p=0.004, $p_{Holm\text{-}Bonferroni}$=0.02), and a trend towards significantly lower qT1 values in older adults at venous distances of 2.01-4 mm compared to younger adults (t(22.878)=1.756, p=0.092). This effect is reversed at venous distances of 8.01-10 mm, where older adults show a trend towards significantly higher qT1 values (lower myelination) compared to younger adults (t(26.499)=-1.745, p=0.093, see **Figure 2E**). This shows that older adults have higher cortical myelination than younger adults close to a vein, but lower cortical myelination than younger adults more distant to a vein.

Critically, the interaction between age and venous distance remains significant when excluding the closest distance of 0.01-2 mm that is most prone to partial volume effects (see **Supplementary Table 2**).

Finally, a significant three-way interaction between age, brain area and venous distance (see **Table 2**) reveals that this effect is mainly driven by M1 rather than S1. More specifically, post hoc *t*-tests reveal significant differences in M1 at venous distances of 0.01-2 mm between younger adults and older adults ($t(21.015)=2.845$, $p=0.010$, $p_{Holm\text{-}Bonferroni}=0.05$), and at venous distances of 8.01-10 mm between younger adults and older adults ($t(33)=-2.276$, $p=0.029$, $p_{Holm\text{-}Bonferroni}=0.116$), whereas in S1, there is only a significant difference at venous distances of 0.01-2 mm between younger adults and older adults ($t(33)=2.701$, $p=0.011$, $p_{Holm\text{-}Bonferroni}=0.05$, see **Figure 2G,H**). Critically, the interaction effect remained significant when excluding the closest distance of 0.01-2 mm (see **Supplementary Table 2**).

Controlling for effects of vascular health, comparisons of multilevel linear regression models (random intercept models) reveal no significant effect of vascular health risk (binary variable indicating the presence of hypertension and/or signs of cerebral small vessel diseases) on qT1 values (M1: $\chi2(1)=1.35$, $p=0.245$; S1: $\chi2(1)=0.25$, $p=0.621$; full model: qT1 ~ distance to vein + vascular risk + 1|participant; reduced model: qT1 ~ distance to vein + 1|participant), and no significant interaction effect between vascular health risk and distance to the nearest vein on qT1 values (M1: $\chi2(5)=5.22$, $p=0.389$; S1: $\chi2(5)=1.70$, $p=0.889$; full model: qT1 ~ distance + vascular risk + distance:vascular risk + 1|participant; reduced model: qT1 ~ distance + 1|participant) in older adults (see **Figure 3** for the distribution of vascular health risk).

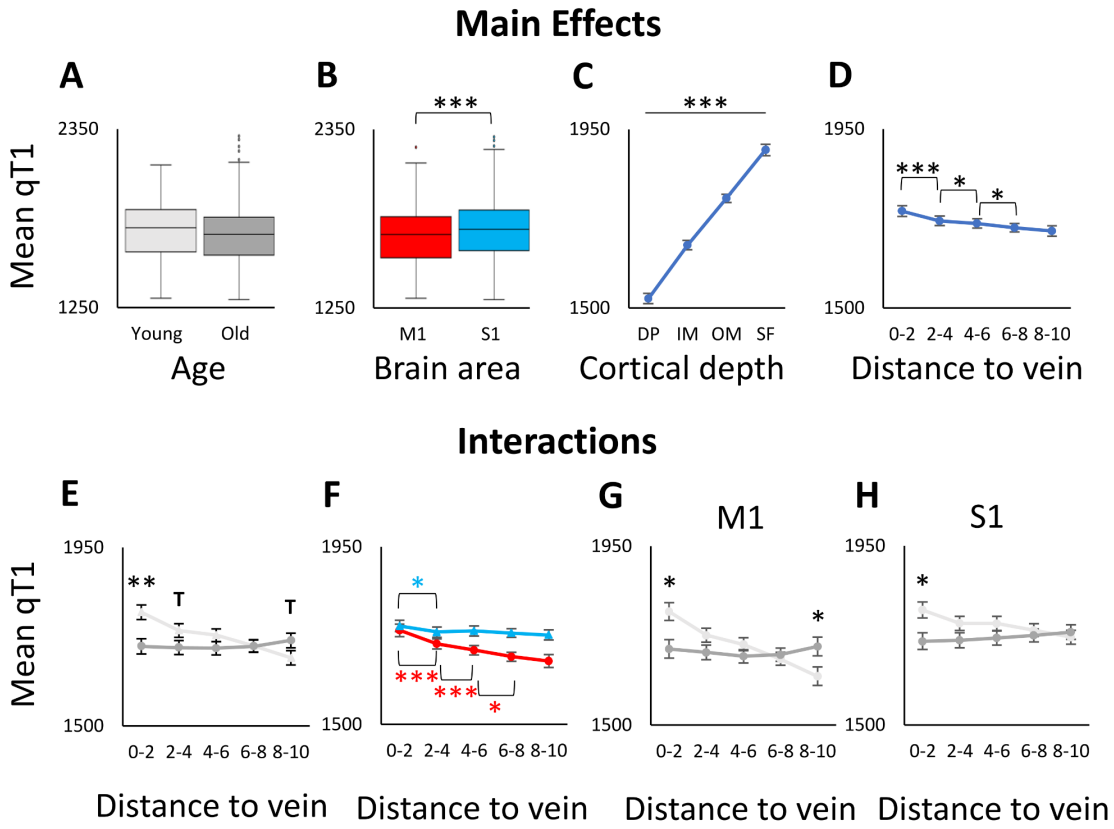

M1	–	Motor cortex	**DP**	–	Deep cortical depth	**0-2**	–	0.01-2 mm distance to vein
S1	–	Sensory cortex	**IM**	–	Inner middle cortical depth	**2-4**	–	2.01-4 mm distance to vein
			OM	–	Outer middle cortical depth	**4-6**	–	4.01-6 mm distance to vein
			SF	–	Superficial cortical depth	**6-8**	–	6.01-8 mm distance to vein
						8-10	–	8.01-10 mm distance to vein

Figure 2. Effects of age, brain area, cortical depth and venous distance on cortical myelination. qT1 values are given in milliseconds (lower values indicate higher myelin content). **A:** Box plots show no significant main effect of age on qT1 values. Shown are medians, interquartile ranges, and lower and upper quartiles for younger (n=18, *light grey*) and older (n=17, *dark grey*) adults. Dots above a box mark outliers. **B:** Box plots show a significant main effect of brain area (i.e., M1 (*red*) and S1 (*blue*)) on qT1 values. **C:** Line graph shows the main effect of cortical depth on qT1 values; dots represent mean qT1 values for the different cortical depths averaged across age groups, distances, and brain areas. Error bars show standard errors of the mean (SEM). **D:** Line graph shows main effect of venous distance on qT1 values (0 - 2 = 0.01 - 2 mm, 2 - 4 = 2.01 - 4 mm, 4 - 6 = 4.01 -6 mm, 6 - 8 = 6.01 - 8 mm, 8 - 10 = 8.01 - 10 mm). **E:** Line graph shows interaction effect between venous distance and age on qT1 values. **F:** Line graphs show interaction effect between venous distance and brain area on qT1 values. **G / H:** Line graphs show interaction effects between venous distance, age and brain area (**G**: data for M1, **H**: data for S1). Significant results are marked by asterisks: * $p \leq 0.05$, ** $p \leq 0.005$, *** $p \leq 0.0005$ (uncorrected). Trends above p=0.05 are marked by a T.

Effect	Conditions	Mean (ms)	SEM (ms)	Statistics				
				DFn	DFd	F	p	η_{G^2}
Age	Young	1725.97	15.94	1	33	1.092	0.304	0.018
	Old	1702.08	16.40					
Brain Area	M1	1692.42	12.71	1	33	24.856	$1.924*10^{-5}$	0.056
	S1	1735.63	11.73					
Cortical depth	Deep	1523.86	13.13	3	31	909.332	$2.285*10^{-37}$	0.708
	Inner Middle	1658.11	11.65					
	Outer Middle	1776.34	10.22					
	Superficial	1897.80	13.98					
Distance	0.01 - 2 mm	1743.83	13.46	4	30	16.289	$9.651*10^{-6}$	0.036
	2.01 - 4 mm	1719.03	12.16					
	4.01 - 6 mm	1712.38	11.53					
	6.01 - 8 mm	1701.47	10.89					
	8.01 - 10 mm	1693.41	12.87					
Age x Distance	Young / 0.01 - 2 mm	1786.91	18.76	4	30	25.657	$7.668*10^{-8}$	0.056
	Young / 2.01 - 4 mm	1740.50	16.95					
	Young / 4.01 - 6 mm	1728.96	16.06					
	Young / 6.01 - 8 mm	1702.08	15.17					
	Young / 8.01 - 10 mm	1671.42	17.94					
	Old / 0.01 - 2 mm	1700.76	19.31					
	Old / 2.01 - 4 mm	1697.57	17.44					
	Old / 4.01 - 6 mm	1695.80	16.53					
	Old / 6.01 - 8 mm	1700.87	15.61					
	Old / 8.01 - 10 mm	1715.39	18.46					
Age x Brain Area	Young / M1	1700.53	17.71	1	33	0.783	0.382	0.002
	Old / M1	1684.31	18.23					
	Young / S1	1751.41	16.36					
	Old / S1	1719.85	16.83					
Brain Area x Distance	M1 / 0.01 - 2 mm	1738.28	16.18	4	30	8.628	$2.325*10^{-4}$	0.013
	M1 / 2.01 - 4 mm	1704.16	12.67					
	M1 / 4.01 - 6 mm	1687.94	11.69					
	M1 / 6.01 - 8 mm	1671.56	11.81					
	M1 / 8.01 - 10 mm	1660.16	16.50					
	S1 / 0.01 - 2 mm	1749.39	14.49					
	S1 / 2.01 - 4 mm	1733.91	12.96					
	S1 / 4.01 - 6 mm	1736.82	12.58					
	S1 / 6.01 - 8 mm	1731.39	11.47					
	S1 / 8.01 - 10 mm	1726.65	12.68					
Age x Brain Area x Distance	Young / M1 / 0.01 - 2 mm	1785.29	22.55	4	30	3.714	0.024	0.006
	Young / M1 / 2.01 - 4 mm	1725.63	17.66					
	Young / M1 / 4.01 - 6 mm	1702.89	16.30					
	Young / M1 / 6.01 - 8 mm	1666.23	16.46					
	Young / M1 / 8.01 - 10 mm	1622.62	23.00					
	Young / S1 / 0.01 - 2 mm	1788.53	20.20					
	Young / S1 / 2.01 - 4 mm	1755.36	18.06					
	Young / S1 / 4.01 - 6 mm	1755.03	17.53					
	Young / S1 / 6.01 - 8 mm	1737.92	15.99					
	Young / S1 / 8.01 - 10 mm	1720.23	17.68					
	Old / M1 / 0.01 - 2 mm	1691.27	23.21					
	Old / M1 / 2.01 - 4 mm	1682.68	18.17					
	Old / M1 / 4.01 - 6 mm	1672.99	16.77					
	Old / M1 / 6.01 - 8 mm	1676.88	16.94					
	Old / M1 / 8.01 - 10 mm	1697.71	23.66					
	Old / S1 / 0.01 - 2 mm	1710.25	20.79					
	Old / S1 / 2.01 - 4 mm	1712.45	18.58					
	Old / S1 / 4.01 - 6 mm	1718.60	18.04					
	Old / S1 / 6.01 - 8 mm	1724.86	16.45					
	Old / S1 / 8.01 - 10 mm	1733.07	18.19					

Table 2. ANOVA Results for qT1 values. Results for the mixed-effects ANOVA on qT1 values with factors age (n=18 younger, n=17 older), cortical depth (SF, OM, IM, DP), brain area (S1, M1) and venous distance (5 distances). Given are mean qT1 values in milliseconds (Mean) and standard error of the mean (SEM), degrees of freedom of the numerator (DFn), degrees of freedom of the denominator (DFd), p-values (p), and effect sizes (n_G^2). P-values below 0.05 are considered as significant.

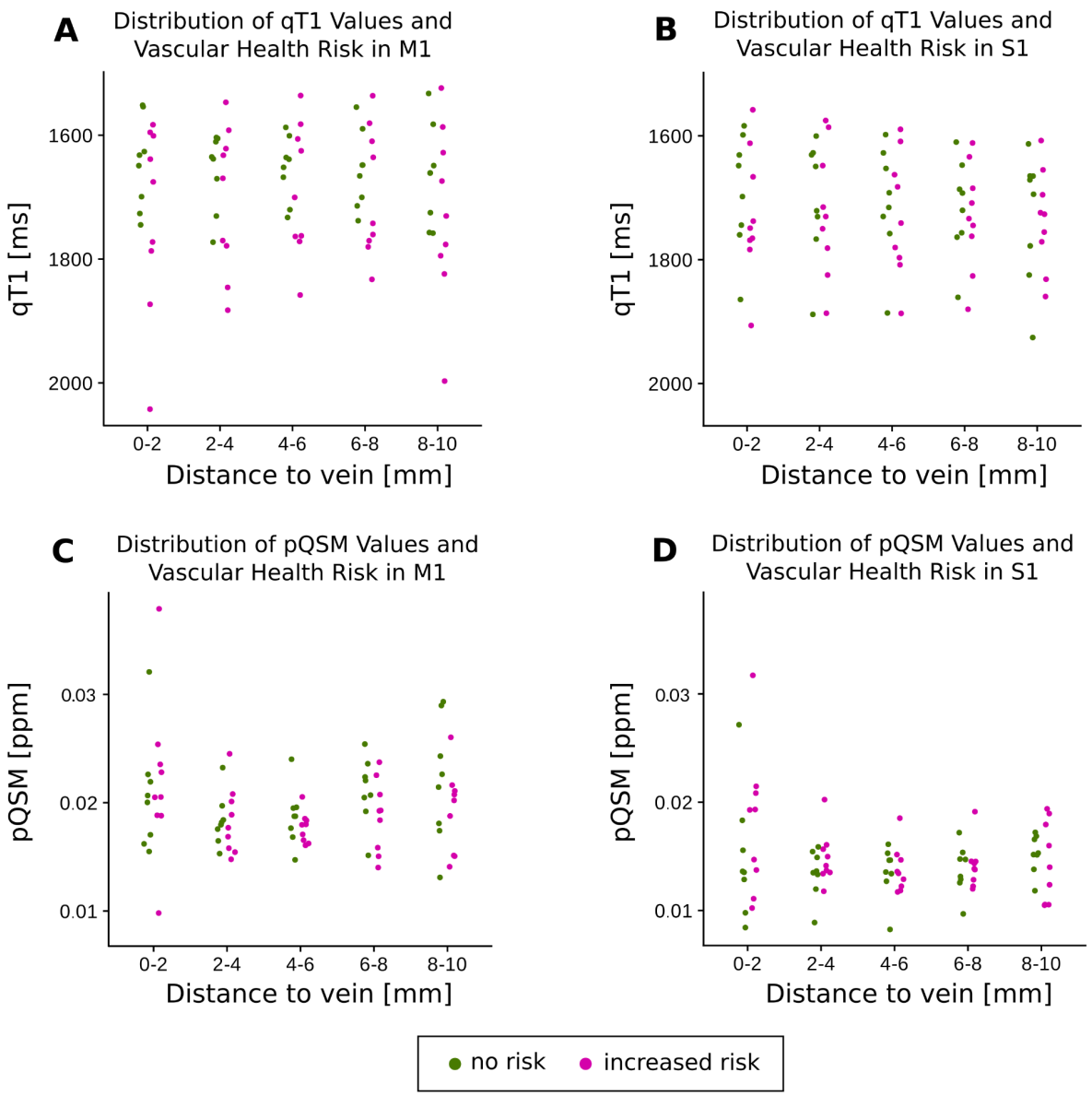

Figure 3. Distribution of vascular health risk in older adults. Individual vascular health risk (i.e., binary variable indicating the presence of hypertension and/or signs of cerebral small vessel diseases according to the STRIVE-2 criteria; green: no risk, magenta: increased risk) shown in relation to the distance to the nearest vein (distance, given in millimetres). (A) Distribution of vascular health risk for older adults (n=17) in primary motor cortex (M1) in relation to quantitative T1 values (qT1, given in milliseconds). (B) Distribution of vascular health risk for older adults in primary somatosensory cortex (S1) in relation to quantitative T1 values (qT1, given in milliseconds). (C) Distribution of vascular health risk for older adults in M1 in relation to positive QSM values (pQSM, given in parts per million, i.e. ppm). (D) Distribution of vascular health risk for older adults in S1 in relation to positive QSM values (pQSM, given in parts per million, i.e. ppm).

3.2. Cortical iron content depends on the distance to the nearest vein

To test for the effect of venous distance on age-related changes in cortical iron content, we computed the same ANOVA on pQSM values. As expected, there is a significant main effect of brain area (see **Table 3**) with higher pQSM values (more iron) in M1 compared to S1 (see **Figure 4B**), and a significant main effect of cortical depth driven by less iron in deeper layers in M1 and S1 (see **Table 3**, **Figure 4C**).

There is also a significant main effect of venous distance (see **Table 3**) driven by significantly higher pQSM values (more iron) at distances 0.01-2 mm compared to distances 2.01-4 mm ($t(34)=4.388$, $p=1.052*10^{-4}$, $p_{Holm\text{-}Bonferroni}=4.208*10^{-4}$, see **Table 3** for means and standard errors of compared conditions), and significantly lower pQSM values (less iron) at distances 4.01-6 mm compared to distances 6.01-8 mm ($t(34)=-6.132$, $p=5.799*10^{-7}$, $p_{Holm\text{-}Bonferroni}=1.740*10^{-6}$) and at distances 6.01-8 mm compared to distances 8.01-10 mm ($t(34)=-2.289$, $p=0.028$, $p_{Holm\text{-}Bonferroni}=0.056$, see **Figure 4D**). There is also a trend towards significantly higher pQSM values at distances 2.01-4 mm compared to distances 4.01-6 mm ($t(34)=1.715$, $p=0.095$). This shows that in both younger and older adults, there is a U-shaped relationship between cortical iron content and venous distance. Other than for cortical myelin, this effect is not mediated by brain area (see **Figure 4F**, **Table 3**).

We then explored potential age effects and detected a significant main effect of age (see **Table 3**) with higher pQSM values (more iron) in older compared to younger adults in both M1 and S1 (see **Figure 4A**). However, other than for cortical myelin, the age effect is not mediated by the distance to the nearest vein (see **Figure 4E, Table 3**); instead, age effects differ significantly between brain areas (see **Table 3**), showing more pronounced age effects in M1 compared to S1 (M1: younger adults - older adults=-0.0067 ppm, $t(33)=-8.860$, $p=4.505*10^{-11}$, $p_{Holm\text{-}Bonferroni}=9.01*10^{-11}$; S1: younger adults - older adults=-0.0026 ppm, $t(33)=-3.416$, $p=0.008$, $p_{Holm\text{-}Bonferroni}=0.008$).

These results are confirmed when excluding the closest distance of 0.01-2 mm, except that in this analysis, there is a significant three-way interaction between age, brain area and venous distance (see **Supplementary Table 3**) driven by the less pronounced U-shaped relationship between pQSM values and venous distance when the closest distance is removed in both age groups (see **Figures 4G,H**). This leads to age-related differences in cortical iron content that are dependent on

the distance to the nearest vein, but this effect is different in M1 versus S1 (M1: more iron in older adults with increasing venous distances (older - younger): 2.01-4 mm=0.0054 ppm, 4.01-6 mm=0.0059 ppm, 6.01-8 mm=0.0072 ppm, 8-10=0.0073 ppm; S1: more iron in older adults with decreasing venous distances (older - younger): 2.01-4 mm=0.0035 ppm, 4.01-6 mm=0.0030 ppm, 6.01-8 mm=0.0016 ppm, 8.01-10 mm=0.0011 ppm). Taken together, age effects on iron content are stronger in M1 compared to S1, and when excluding the closest distance, it becomes apparent that iron accumulation in older adults is stronger at distances farther away from a vein in M1 and closer to a vein in S1.

Controlling for effects of vascular health, a simple linear regression revealed no significant effect of vascular health risk (binary variable indicating the presence of hypertension and/or signs of cerebral small vessel diseases) on pQSM values in older adults, neither for M1 (b=-0.001 ppm, $t(15)$=-0.76, p=0.459, R^2=0.037) nor for S1 (b=0.0009 ppm, $t(15)$=0.77, p=0.454, R^2=0.038).

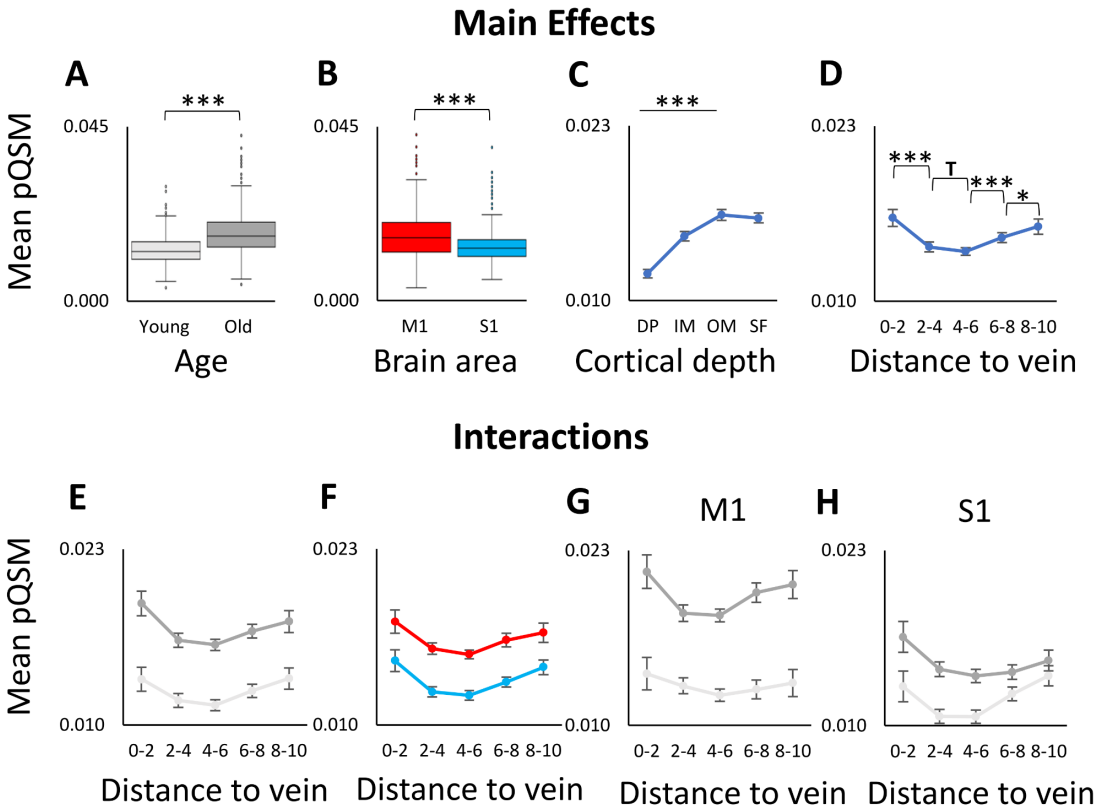

M1	–	Motor cortex	**DP**	–	Deep cortical depth	**0-2**	–	0.01-2 mm distance to vein
S1	–	Sensory cortex	**IM**	–	Inner middle cortical depth	**2-4**	–	2.01-4 mm distance to vein
			OM	–	Outer middle cortical depth	**4-6**	–	4.01-6 mm distance to vein
			SF	–	Superficial cortical depth	**6-8**	–	6.01-8 mm distance to vein
						8-10	–	8.01-10 mm distance to vein

Figure 4. Effects of age, brain region, cortical depth and venous distance on pQSM values. A: Box plots show the main effect of age on pQSM values. Shown are medians, interquartile ranges, and lower and upper quartiles for younger (n=18, *light grey*) and older (n=17, *dark grey*) adults. Dots mark outliers. pQSM values are given in ppm (higher values indicate higher iron content). **B:** Box plots show the main effect of brain area (M1 (*red*) versus S1 (*blue*)) on pQSM values. **C:** The line graph shows the main effect of cortical depth on pQSM values. Dots indicate mean pQSM values for different cortical depths averaged across age groups, distances, and brain areas. Error bars indicate standard errors of the mean (SEM). **D:** The line graph shows the main effect of venous distance on pQSM values (0-2 = 0.01- 2 mm, 2-4 = 2.01-4 mm, 4-6 = 4.01-6 mm, 6-8 = 6.01-8 mm, 8-10 = 8.01-10 mm). **E:** The line graph shows the interaction effect between venous distance and age on pQSM values. **F:** The line graph shows the interaction effect between venous distance and brain area on pQSM values. **G / H:** Line graphs show the interaction effect between venous distance, age and brain area (G: data for M1, H: data for S1). Significant results are marked by asterisks: * $p \leq 0.05$, ** $p \leq 0.005$, *** $p \leq 0.0005$ (uncorrected). Trends above $p=0.05$ are marked by a T.

Effect	Conditions	Mean (ppm)	SEM (ppm)	Statistics				
				DFn	DFd	F	p	η_G^2
Age	Young	0.0125	0.00046	1	33	48.395	$5.954*10^{-8}$	0.270
	Old	0.0172	0.00048					
Brain Area	M1	0.0163	0.00039	1	33	69.291	$1.292*10^{-9}$	0.131
	S1	0.0134	0.00036					
Cortical depth	Deep	0.0120	0.00032	3	31	152.340	$1.384*10^{-24}$	0.172
	Inner Middle	0.0148	0.00035					
	Outer Middle	0.0164	0.00041					
	Superficial	0.0162	0.00036					
Distance	0.01 - 2 mm	0.0162	0.00063	4	30	8.366	0.002	0.056
	2.01 - 4 mm	0.0140	0.00037					
	4.01 - 6 mm	0.0137	0.00029					
	6.01 - 8 mm	0.0147	0.00036					
	8.01 - 10 mm	0.0155	0.00057					
Age x Distance	Young / 0.01 - 2 mm	0.0134	0.00088	4	30	0.612	0.508	0.004
	Young / 2.01 - 4 mm	0.0118	0.00051					
	Young / 4.01 - 6 mm	0.0115	0.00040					
	Young / 6.01 - 8 mm	0.0125	0.00050					
	Young / 8.01 - 10 mm	0.0134	0.00079					
	Old / 0.01 - 2 mm	0.0190	0.00090					
	Old / 2.01 - 4 mm	0.0163	0.00052					
	Old / 4.01 - 6 mm	0.0159	0.00042					
	Old / 6.01 - 8 mm	0.0169	0.00051					
	Old / 8.01 - 10 mm	0.0177	0.00082					
Age x Brain Area	Young / M1	0.0129	0.00055	1	33	33.449	$1.825*10^{-6}$	0.068
	Old / M1	0.0197	0.00056					
	Young / S1	0.0121	0.00050					
	Old / S1	0.0147	0.00052					
Brain Area x Distance	M1 / 0.01 - 2 mm	0.0176	0.00087	4	30	0.185	0.790	0.001
	M1 / 2.01 - 4 mm	0.0156	0.00042					
	M1 / 4.01 - 6 mm	0.0152	0.00032					
	M1 / 6.01 - 8 mm	0.0163	0.00050					
	M1 / 8.01 - 10 mm	0.0168	0.00072					
	S1 / 0.01 - 2 mm	0.0147	0.00080					
	S1 / 2.01 - 4 mm	0.0124	0.00038					
	S1 / 4.01 - 6 mm	0.0122	0.00035					
	S1 / 6.01 - 8 mm	0.0132	0.00037					
	S1 / 8.01 - 10 mm	0.0143	0.00053					
Age x Brain Area x Distance	Young / M1 / 0.01 - 2 mm	0.0138	0.00121	4	30	2.293	0.120	0.011
	Young / M1 / 2.01 - 4 mm	0.0129	0.00059					
	Young / M1 / 4.01 - 6 mm	0.0122	0.00045					
	Young / M1 / 6.01 - 8 mm	0.0127	0.00070					
	Young / M1 / 8.01 - 10 mm	0.0132	0.00101					
	Young / S1 / 0.01 - 2 mm	0.0129	0.00112					
	Young / S1 / 2.01 - 4 mm	0.0107	0.00052					
	Young / S1 / 4.01 - 6 mm	0.0107	0.00049					
	Young / S1 / 6.01 - 8 mm	0.0124	0.00051					
	Young / S1 / 8.01 - 10 mm	0.0137	0.00074					
	Old / M1 / 0.01 - 2 mm	0.0214	0.00125					
	Old / M1 / 2.01 - 4 mm	0.0183	0.00061					
	Old / M1 / 4.01 - 6 mm	0.0182	0.00046					
	Old / M1 / 6.01 - 8 mm	0.0199	0.00072					
	Old / M1 / 8.01 - 10 mm	0.0205	0.00104					
	Old / S1 / 0.01 - 2 mm	0.0166	0.00115					
	Old / S1 / 2.01 - 4 mm	0.0142	0.00054					
	Old / S1 / 4.01 - 6 mm	0.0137	0.00051					
	Old / S1 / 6.01 - 8 mm	0.0140	0.00053					
	Old / S1 / 8.01 - 10 mm	0.0148	0.00077					

Table 3. ANOVA Results for pQSM values. Results for the ANOVA on pQSM values with factors age (n=18 younger, n=17 older), cortical depth (SF, OM, IM, DP), brain area (S1, M1) and venous distance (5 distances). Given are mean qT1 values in milliseconds (Mean) and standard error of the mean (SEM), degrees of freedom of the numerator (DFn), degrees of freedom of the denominator (DFd), p-values (p), and effect sizes (n_G^2). P-values below 0.05 are considered as significant.

4. Discussion

We here provide insights that the distance to the nearest vein is related to age-related differences in cortical microstructure. Specifically, we tested three hypotheses: Cortical locations that are *more distant* to the next larger blood vessel are more prone to age-related structural alterations (H1), cortical locations that are *closer* to the next larger blood vessel are more prone to age-related structural alterations (H2), age-related cortical degeneration is *independent* of the distance to the next blood vessel (H3). Our data confirm H1 for cortical myelin and H3 for cortical iron. In addition, our data shows that in both younger and older adults, there is a linear negative relation between cortical myelination and venous distance, and a U-shaped relation between cortical iron and venous distance. Together, this data shows that the local venous architecture explains a significant amount of variance in standard measures of cortical microstructure in younger adults and older adults, and needs to be considered in neurobiological models of human brain organisation and cortical ageing.

We report a significant interaction between age and venous distance on qT1 values (reflecting cortical myelination). This effect is driven by older adults showing lower qT1 values (more myelin) than younger adults in voxels closer to a vein, but showing a trend towards higher qT1 values (less myelin) in voxels farther away from a vein. Prior studies show either reduced or higher cortical myelination in older compared to younger adults (Seiler et al. 2020; Cho et al. 1997; Grydeland et al. 2013; Grydeland et al. 2019; Callaghan et al. 2014) or no significant differences at all (Northall et al. 2023a). Those contrary findings may be related to hidden variables that explain a significant amount of variance but have been disregarded so far. Our data indicate that the venous architecture, specifically the distance to the nearest vein, acts as such a hidden variable, and that age-related myelin loss specifically occurs more distant from a vein (confirming H1). Given the pQSM effect is reversed (more iron accumulation in older adults in M1 at voxels more distant from a vein), the myelin effect is unlikely to be driven by microvessels that increase pQSM values. Possible neuronal mechanisms driving the distance-dependent myelin loss in ageing are that increased metabolism close to blood vessels may prevent age-related myelin loss, and/or ageing blood vessels particularly reduce supply to locations that are farther away from major branches. Myelin itself can be a driver for increased metabolism, since it is a highly demanding structure (Hirrlinger & Nave, 2014). The venous architecture would in this view be a protective mechanism for older adults' cortical microstructure, specifically with respect

to myelin loss. Perosa et al. (2020) hypothesised that in the hippocampus, a steady arterial vascular supply constitutes a 'vascular reserve' mechanism in cases of pathology, relating to larger hippocampal volume (Vockert et al. 2021) and preserved cognitive abilities in patients with cerebral small vessel disease (Pohlack et al., 2014). Our study indicates that a similar vascular reserve mechanism can be assigned to veins.

Our data shows that the dependence of age-related myelin changes on the distance to the nearest vein is mainly driven by M1 and to a lesser extent by S1. The reason for this difference is at present unclear. Given S1 has significantly higher qT1 values (less myelin) and significantly lower pQSM values (less iron) than M1, one could assume that possible effects of the venous distance on S1 microstructure are harder to detect. Alternatively, the effect of the venous architecture on cortical microstructure might be particularly strong in a motor output area with a pronounced layer V and high cell and myelin density. M1 is more metabolically active than S1 because of its cell structure and function, and may need a much faster turnover of metabolites, thus depending more on intact vessel function.

Such a relationship between age-dependent alterations in cortical microstructure and venous distance, as described above for cortical myelin, cannot be detected for iron, in principle confirming H3. Both younger and older adults show a U-shaped relationship between pQSM values (iron) and venous distances, driven by highest pQSM values (most iron) at cortical voxels closest and farthest away from a vein. This was not modulated by age. However, methodological limitations need to be considered: We here focus on veins at the mesoscopic scale (resolution: 0.5 mm isotropic), and we cannot comment on microvessels below that resolution. Therefore, it is possible that microvessels located close to larger veins increase pQSM values close to larger veins (i.e., at distances 0.01-2 mm). Increased pQSM values at distances close to a vein need to be treated with caution and could potentially be driven by partial volume artefacts. Therefore, we recalculated all analyses taking out the closest distance. When doing so, the cortical myelin effects as described above do not change, but there is an interaction between age, brain area, and venous distance on pQSM values. This is driven by opposing relationships between age-related iron accumulation and venous distance in M1 versus S1: Whereas age-related iron accumulation is larger at greater distances in M1, it is larger at smaller distances in S1. This would confirm H1 and H2 for M1 and S1, respectively, rather than confirming H3. Given the resolution was 0.5 mm isotropic, which limited the amount of small veins that could be classified, the present data can

not completely clarify the relationship between age-related iron accumulation and venous distance, but warrant further research in this area using even higher resolutions (i.e., 0.35 mm resolution or higher; van Gelderen et al. 2023). However, if future studies confirm H1 in M1 also for iron accumulation, this would strengthen the argument that the vascular architecture acts as protective mechanisms in ageing.

With respect to study limitations, the participant number was relatively low but motivated by previous layer-dependent 7T MRI studies using quantitative in-vivo proxies to describe the microstructural cortex architecture (Dinse et al., 2015, Kuehn et al., 2017), and is well above previously reported sample sizes. To reduce type I errors, we restricted the number of statistical tests to the minimum number needed (i.e., two ANOVAs and two regression analyses). Moreover, the image resolution of 0.5 mm isotropic did not allow to identify the entire venous network, as already pointed out above. Furthermore, for a comprehensive investigation of the neuronal mechanisms that underlie the interaction between blood vessels and cortical microstructure, also the arterial blood supply patterns need to be investigated, and should be complemented by blood flow assessments. Additional analyses of time-of-flight MRI measurements would benefit future studies. Moreover, previous studies pointed out that hypertension and alterations in brain vasculature relate to myelin loss and M1 pathology (Jacków-Nowicka et al. 2021; Tsushima, et al. 2003; Dobrynina et al. 2018, Li et al. 2023; Schreiber et al. 2023). Here, 9/17 older adults showed global signs of vascular health risk (i.e., presence of hypertension and/or signs of cerebral small vessel diseases outside S1 and M1). However, these indicators did not significantly predict S1 and M1 microstructure in older adults, and may therefore not account for the main findings. We instead argue in favour of a protective mechanism of veins preserving the myeloarchitecture in older age, which may only hold in cases of intact local vascular architecture. Assessing the potential impact of hypertension and other vascular disorders on cortical microstructure is an important topic for future studies.

Taken together, we show that the venous architecture interacts with cortical microstructure and age-related changes thereof. This is an important insight as most studies do not analyse cortical alterations as a function of venous or arterial distance, which may lead to misinterpretations of present (or absent) effects. Our study provides evidence for the importance of the human venous architecture in understanding cortical function in health and disease.

Data availability

MRI data available upon request, requirements are a formal data sharing agreement, the need to submit a formal project outline and co-authorship or inclusion in the author byline.

Code availability

Code for small vessel segmentation hysteresis thresholding: https://gitlab.com/hmattern/omelette

Funding

CK was supported by ESIF/ESF 2014-2020**;** FKZ: ZS/2020/05/141591, Purpose: ZOOM-IN. The project was supported by the German Research Foundation (DFG) project number 425899996 – SFB 1436. HM was supported by the German Research Foundation (DFG) project number MA 9235/1-1 (446268581) and MA 9235/3-1 (501214112). AN was supported by the Else Kröner Fresenius Stiftung: 2019-A03. JD was funded by the German Research Foundation (DFG) (KU 3711/2-1, project number: 423633679 and project-ID 425899996 – SFB 1436).

Competing interests

The authors report no competing interests.

Author contributions

Christoph Knoll: Formal analysis, Investigation, Writing Original Draft **Juliane Doehler:** Data collection, Formal analysis, Methodology, Investigation, Writing -review & editing **Alicia Northall:** Formal analysis, Methodology, Writing -review & editing **Stefanie Schreiber:** Conceptualization, Writing -review & editing **Johanna Rotta:** Formal analysis **Hendrik Mattern:** Methodology, Software, Writing -review & editing **Esther Kuehn:** Conceptualization, Investigation, Funding acquisition, Supervision, Writing -review & editing.

References

Acosta-Cabronero, J., Betts, M. J., Cardenas-Blanco, A., Yang, S., & Nestor, P. J. (2016). In Vivo MRI Mapping of Brain Iron Deposition across the Adult Lifespan. The Journal of neuroscience : the official journal of the Society for Neuroscience, 36(2), 364–374. https://doi.org/10.1523/JNEUROSCI.1907-15.2016.

Acosta-Cabronero, J., Milovic, C., Mattern, H., Tejos, C., Speck, O., & Callaghan, M. F. (2018). A robust multi-scale approach to quantitative susceptibility mapping. Neuroimage, 183, 7-24. https://doi.org/10.1016/j.neuroimage.2018.07.065.

Arenaza-Urquijo, E. M., Przybelski, S. A., Lesnick, T. L., Graff-Radford, J., Machulda, M. M., Knopman, D. S., Schwarz, C. G., Lowe, V. J., Mielke, M. M., Petersen, R. C., Jack, C. R., & Vemuri, P. (2019). The metabolic brain signature of cognitive resilience in the 80+: beyond Alzheimer pathologies. Brain: A Journal of Neurology, 142(4), 1134–1147.

Avants, B. B., Tustison, N. J., Song, G., Cook, P. A., Klein, A., & Gee, J. C. (2011). A reproducible evaluation of ANTs similarity metric performance in brain image registration. NeuroImage, 54 (3), 2033–2044. doi:10.1016/j.neuroimage.2010.09.025.

Bazin, P. L. & Pham, D. L. (2007). Topology-preserving tissue classification of magnetic resonance brain images. IEEE transactions on medical imaging, 26(4), 487-496.

Bazin, P. L., Plessis, V., Fan, A. P., Villringer, A., & Gauthier, C. J. (2016). Vessel segmentation from quantitative susceptibility maps for local oxygenation venography. In 2016 IEEE International Symposium on Biomedical Imaging: From Nano to Macro, ISBI 2016 - Proceedings (pp. 1135-1138). [7493466] (Proceedings - International Symposium on Biomedical Imaging; Vol. 2016-June). IEEE Computer Society. https://doi.org/10.1109/ISBI.2016.7493466.

Bazin, P. L., Weiss, M., Dinse, J., Schäfer, A., & Trampel, R. (2014). A computational framework for ultra-high resolution cortical segmentation at 7 Tesla. NeuroImage, 93, 201–209. doi:10.1016/j.neuroimage.2013.03.077.

Bernier, M., Cunnane, S. C., & Whittingstall, K. (2018). The morphology of the human cerebrovascular system. Human brain mapping, 39(12), 4962–4975. https://doi.org/10.1002/hbm.24337.

Betts, M. J., Acosta-Cabronero, J., Cardenas-Blanco, A., Nestor, P. J., & Düzel, E. (2016). High-resolution characterisation of the aging brain using simultaneous quantitative susceptibility mapping (QSM) and R2* measurements at 7T. NeuroImage, 138, 43–63. https://doi.org/10.1016/j.neuroimage.2016.05.024.

Brainard D. H. (1997). The Psychophysics Toolbox. Spatial vision, 10(4), 433–436.

Callaghan, M. F., Freund, P., Draganski, B., Anderson, E., Cappelletti, M., Chowdhury, R., Diedrichsen, J., Fitzgerald, T. H. B., Smittenaar, P., Helms, G., Lutti, A., & Weiskopf, N. (2014). Widespread age-related differences in the human brain microstructure revealed by quantitative magnetic resonance imaging. Neurobiology of Aging, 35(8), 1862–1872.

Chen, J., Zhang, Z., Nie, X., Xu, Y., Liu, C., Zhao, X., Miao, Z., Wang, Y., & Liu, L. (2022). Thrombus magnetic susceptibility is associated with recanalization and clinical outcome in patients with ischemic stroke. NeuroImage. Clinical, 36, 103183. https://doi.org/10.1016/j.nicl.2022.103183.

Cho, S., Jones, D., Reddick, W. E., Ogg, R. J., & Steen, R. G. (1997). Establishing norms for age-related changes in proton T1 of human brain tissue in vivo. Magnetic resonance imaging, 15(10), 1133–1143. https://doi.org/10.1016/s0730-725x(97)00202-6.

Cohen, J. (1988). Statistical Power Analysis for the Behavioral Sciences (2nd Edition). Routledge.

Denk, C. & Rauscher, A. (2010). Susceptibility weighted imaging with multiple echoes. Journal of magnetic resonance imaging: JMRI, 31(1), 185–191. https://doi.org/10.1002/jmri.21995.

Deistung, A., Schäfer, A., Schweser, F., Biedermann, U., Turner, R., & Reichenbach, J. R. (2013). Toward in vivo histology: a comparison of quantitative susceptibility mapping (QSM) with magnitude-, phase-, and R2∗-imaging at ultra-high magnetic field strength. Neuroimage, 65, 299-314.

Dinse, J., Härtwich, N., Waehnert, M. D., Tardif, C. L., Schäfer, A., Geyer, S., Preim, B., Turner, R., & Bazin, P. L. (2015). A cytoarchitecture-driven myelin model reveals area-specific signatures in human primary and secondary areas using ultra-high resolution in-vivo brain MRI.

NeuroImage, 114, 71–87. https://doi.org/10.1016/j.neuroimage.2015.04.023.

Dobrynina, L. A., Zabitova, M. R., Kalashnikova, L. A., Gnedovskaya, E. V., & Piradov, M. A. (2018). Hypertension and Cerebral Microangiopathy (Cerebral Small Vessel Disease): Genetic and Epigenetic Aspects of Their Relationship. Acta naturae, 10(2), 4–15.

Doehler, J., Northall, A., Liu, P., Fracasso, A., Chrysidou, A., Speck, O., Lohmann, G., Wolbers, T., & Kuehn, E. (2023). The 3D Structural Architecture of the Human Hand Area is Non-Topographic. The Journal of Neuroscience: The Official Journal of the Society for Neuroscience. https://doi.org/10.1523/JNEUROSCI.1692-22.2023.

Duering, M., Biessels, G. J., Brodtmann, A., Chen, C., Cordonnier, C., de Leeuw, F. E., Debette, S., Frayne, R., Jouvent, E., Rost, N. S., Ter Telgte, A., Al-Shahi Salman, R., Backes, W. H., Bae, H. J., Brown, R., Chabriat, H., De Luca, A., deCarli, C., Dewenter, A., Doubal, F. N., … Wardlaw, J. M. (2023). Neuroimaging standards for research into small vessel disease-advances since 2013. The Lancet. Neurology, 22(7), 602–618. https://doi.org/10.1016/S1474-4422(23)00131-X.

Elbert, T., Pantev, C., Wienbruch, C., Rockstroh, B., & Taub, E. (1995). Increased cortical representation of the fingers of the left hand in string players. Science, 270(5234), 305–307.

Farkas, E., de Vos, R. A. I., Donka, G., Jansen Steur, E. N., Mihály, A., & Luiten, P. G. M. (2006). Age-related microvascular degeneration in the human cerebral periventricular white matter. Acta Neuropathologica, 111(2), 150–157.

Flechsig, P. (1901) Developmental (myelogenetic) localisation of the cerebral cortex in the human subject. Lancet 2, 1027–1029. https://doi.org/10.1016/S0140-6736(01)01429-5.

Fraz, M. M., Basit, A., Remagnino, P., Hoppe, A., Barman, S. A. (2011). Retinal vasculature segmentation by morphological curvature, reconstruction and adapted hysteresis thresholding [Internet]. In: 7th International Conference on Emerging Technologies (ICET); Islamabad, Pakistan. Piscataway, NJ:IEEE; 2011. p. 1–6.

Garcia-Garcia, B., Mattern, H., Vockert, N., Yakupov, R., Schreiber, F., Spallazzi, M., Perosa, V., Haghikia, A., Speck, O., Düzel, E., Maass, A., & Schreiber, S. (2023). Vessel Distance Mapping: A novel methodology for assessing vascular-induced cognitive resilience.

NeuroImage, 120094.

van Gelderen, P., Li, X., de Zwart, J. A., Beck, E. S., Okar, S. V., Huang, Y., ... & Liu, J. (2023). Effect of motion, cortical orientation and spatial resolution on quantitative imaging of cortical R2* and magnetic susceptibility at 0.3 mm in-plane resolution at 7 T. NeuroImage, 270, 119992.

Gescheider, G. A., Zwislocki, J. J., & Rasmussen, A. (1996). Effects of stimulus duration on the amplitude difference limen for vibrotaction. The Journal of the Acoustical Society of America, 100(4 Pt 1), 2312–2319. https://doi.org/10.1121/1.417940.

Geyer, S., Schleicher, A., & Zilles, K. (1999). Areas 3a, 3b, and 1 of Human Primary Somatosensory Cortex: 1. Microstructural Organization and Interindividual Variability. NeuroImage, 10 (1), 63–83. doi:10.1006/NIMG.1999.0440.

Glasser, M. F., & Van Essen, D. C. (2011). Mapping human cortical areas in vivo based on myelin content as revealed by T1- and T2-weighted MRI. The Journal of neuroscience : the official journal of the Society for Neuroscience, 31(32), 11597–11616. https://doi.org/10.1523/JNEUROSCI.2180-11.2011.

Glasser, M. F., Coalson, T. S., Robinson, E. C., Hacker, C. D., Harwell, J., Yacoub, E., Ugurbil, K., Andersson, J., Beckmann, C. F., Jenkinson, M., Smith, S. M., & Van Essen, D. C. (2016). A multi-modal parcellation of human cerebral cortex. Nature, 536(7615), 171–178. https://doi.org/10.1038/nature18933.

Grydeland, H., Walhovd, K. B., Tamnes, C. K., Westlye, L. T., & Fjell, A. M. (2013). Intracortical myelin links with performance variability across the human lifespan: results from T1- and T2-weighted MRI myelin mapping and diffusion tensor imaging. The Journal of neuroscience : the official journal of the Society for Neuroscience, 33(47), 18618–18630. https://doi.org/10.1523/JNEUROSCI.2811-13.2013.

Grydeland, H., Vértes, P. E., Váša, F., Romero-Garcia, R., Whitaker, K., Alexander-Bloch, A. F., Bjørnerud, A., Patel, A. X., Sederevicius, D., Tamnes, C. K., Westlye, L. T., White, S. R., Walhovd, K. B., Fjell, A. M., & Bullmore, E. T. (2019). Waves of Maturation and Senescence in Micro-structural MRI Markers of Human Cortical Myelination over the Lifespan. Cerebral cortex (New York, N.Y. : 1991), 29(3), 1369–1381. https://doi.org/10.1093/cercor/bhy330.

Gryga, M., Taubert, M., Dukart, J., Vollmann, H., Conde, V., Sehm, B., Villringer, A., & Ragert, P. (2012). Bidirectional gray matter changes after complex motor skill learning. Frontiers in systems neuroscience, 6, 37. https://doi.org/10.3389/fnsys.2012.00037

Guntupalli, J. S., Hanke, M., Halchenko, Y. O., Connolly, A. C., Ramadge, P. J., & Haxby, J. V. (2016). A Model of Representational Spaces in Human Cortex. Cerebral cortex (New York, N.Y. : 1991), 26(6), 2919–2934. https://doi.org/10.1093/cercor/bhw068.

Haacke, E. M., Xu, Y., Cheng, Y. C. N., & Reichenbach, J. R. (2004). Susceptibility weighted imaging (SWI). Magnetic Resonance in Medicine: An Official Journal of the International Society for Magnetic Resonance in Medicine, 52(3), 612-618.

Haast, R. A., Ivanov, D., Formisano, E., & Uludağ, K. (2016). Reproducibility and reliability of quantitative and weighted T1 and T2* mapping for myelin-based cortical parcellation at 7 Tesla. Frontiers in neuroanatomy, 10, 112.

Hametner, S., Endmayr, V., Deistung, A., Palmrich, P., Prihoda, M., Haimburger, E., ... & Grabner, G. (2018). The influence of brain iron and myelin on magnetic susceptibility and effective transverse relaxation-A biochemical and histological validation study. *Neuroimage*, *179*, 117-133.

Han, X., Pham, D. L., Tosun, D., Rettmann, M. E., Xu, C., & Prince, J. L. (2004). CRUISE: Cortical reconstruction using implicit surface evolution. NeuroImage, 23 (3), 997–1012. doi:10.1016/j.neuroimage.2004.06.043.

Hirrlinger, J., & Nave, K. A. (2014). Adapting brain metabolism to myelination and long-range signal transduction. Glia, 62(11), 1749–1761. https://doi.org/10.1002/glia.22737

Huck, J., Wanner, Y., Fan, A. P., Jäger, A.-T., Grahl, S., Schneider, U., et al. (2019). High resolution atlas of the venous brain vasculature from 7 T quantitative susceptibility maps. Brain Structure & Function. doi:10.1007/s00429-019-01919-4.

Jacków-Nowicka, J., Podgórski, P., Bladowska, J., Szcześniak, D., Rymaszewska, J., Zatońska, K., Połtyn-Zaradna, K., Szuba, A., Sa Siadek, M., & Zimny, A. (2021). The Impact of Common Epidemiological Factors on Gray and White Matter Volumes in Magnetic Resonance Imaging-Is Prevention of Brain Degeneration Possible?. Frontiers in neurology, 12, 633619.

https://doi.org/10.3389/fneur.2021.633619.

Kalisch, T., Ragert, P., Schwenkreis, P., Dinse, H. R., & Tegenthoff, M. (2009). Impaired tactile acuity in old age is accompanied by enlarged hand representations in somatosensory cortex. Cerebral cortex (New York, N.Y. : 1991), 19(7), 1530–1538. https://doi.org/10.1093/cercor/bhn190.

Kalisch, T., Tegenthoff, M., & Dinse, H. R. (2008). Improvement of sensorimotor functions in old age by passive sensory stimulation. Clinical interventions in aging, 3(4), 673–690. https://doi.org/10.2147/cia.s3174.

Kuehn, E., Dinse, J., Jakobsen, E., Long, X., Schäfer, A., Bazin, P. L., Villringer, A., Sereno, M. I., & Margulies, D. S. (2017). Body Topography Parcellates Human Sensory and Motor Cortex. Cerebral cortex (New York, N.Y.: 1991), 27(7), 3790–3805. https://doi.org/10.1093/cercor/bhx026.

Kuehn, E., Doehler, J., & Pleger, B. (2017). The influence of vision on tactile Hebbian learning. Scientific reports, 7(1), 9069. https://doi.org/10.1038/s41598-017-09181-6.

Lakens, D. (2013). Calculating and reporting effect sizes to facilitate cumulative science: a practical primer for t-tests and ANOVAs. Frontiers in Psychology, 4, 863.

Li, H., Jacob, M. A., Cai, M., Duering, M., Chamberland, M., Norris, D. G., Kessels, R. P. C., de Leeuw, F. E., Marques, J. P., & Tuladhar, A. M. (2023). Regional cortical thinning, demyelination, and iron loss in cerebral small vessel disease. Brain : a journal of neurology, awad220. Advance online publication. https://doi.org/10.1093/brain/awad220

Langkammer C, Schweser F, Krebs N, Deistung A, Goessler W, Scheurer E, Sommer K, Reishofer G, Yen K, Fazekas F, Ropele S, Reichenbach JR (2012) Quantitative susceptibility mapping (QSM) as a means to measure brain iron? A post mortem validation study. Neuroimage 62:1593–1599. 10.1016/j.neuroimage.2012.05.049.

Lucas, B. C., Bogovic, J. A., Carass, A., Bazin, P. L., Prince, J. L., Pham, D. L., & Landman, B. A. (2010). The Java Image Science Toolkit (JIST) for rapid prototyping and publishing of neuroimaging software. Neuroinformatics, 8(1), 5-17. https://doi.org/10.1007/s12021-009-9061-2.

Lüsebrink, F., Wollrab, A., & Speck, O. (2013). Cortical thickness determination of the human brain using high resolution 3T and 7T MRI data. NeuroImage, 70, 122-131. https://doi.org/10.1016/j.neuroimage.2012.12.016.

Marques, J. P., Kober, T., Krueger, G., van der Zwaag, W., Van de Moortele, P. F., Gruetter, R. (2010). MP2RAGE, a self bias-field corrected sequence for improved segmentation and T1-mapping at high field. NeuroImage, 49 (2), 1271–1281. doi:10.1016/j.neuroimage.2009.10.002.

Mattern, H. (2021a). Vessel distance mapping of the aging subcortical venous vasculature; 37th Annual Scientific Meeting of European Society for Magnetic Resonance in Medicine and Biology. ESMRMB, doi: 10.1007/s10334-021- 00947-8.

Mattern, H. (2021b). Openly available sMall vEsseL sEgmenTaTion pipelinE (OMELETTE); 29th Annual Meeting of International Society of Magnetic Resonance in Medicine. ISMRM, virtual meeting.

Maurer, C. R., Qi, R., Raghavan, V. (2003). A linear time algorithm for computing exact Euclidean distance transforms of binary images in arbitrary dimensions. IEEETrans. Pattern Anal. Mach. Intell., 265–270 doi: 10.1109/TPAMI.2003.1177156.

Mücke, M., Cuhls, H., Radbruch, L., Baron, R., Maier, C., Tölle, T., Treede, R. D., & Rolke, R. (2014). Quantitative sensorische Testung [Quantitative sensory testing]. Schmerz (Berlin, Germany), 28(6), 635–648. https://doi.org/10.1007/s00482-014-1485-4.

Nasreddine, Z. S., Phillips, N. A., Bédirian, V., Charbonneau, S., Whitehead, V., Collin, I., Cummings, J. L., & Chertkow, H. (2005). The Montreal Cognitive Assessment, MoCA: a brief screening tool for mild cognitive impairment. Journal of the American Geriatrics Society, 53(4), 695–699.

Northall, A., Doehler, J., Weber, M., Vielhaber, S., Schreiber, S., & Kuehn, E. (2023a). Layer-Specific Vulnerability is a Mechanism of Topographic Map Aging. Neurobiology of Aging. https://doi.org/10.1016/j.neurobiolaging.2023.04.002.

Northall, A., Doehler, J., Weber, M., Tellez, I., Petri, S., Prudlo, J., Vielhaber, S., Schreiber, S., & Kuehn, E. (2023b). Multimodal layer modelling reveals in vivo pathology in amyotrophic

lateral sclerosis. Brain : a journal of neurology, awad351. Advance online publication. https://doi.org/10.1093/brain/awad351

Oldfield, R. C. (1971). The assessment and analysis of handedness: the Edinburgh inventory. Neuropsychologia, 9(1), 97–113.

Perosa, V., Priester, A., Ziegler, G., Cardenas-Blanco, A., Dobisch, L., Spallazzi, M., Assmann, A., Maass, A., Speck, O., Oltmer, J., Heinze, H. J., Schreiber, S., Düzel, E. (2020). Hippocampal vascular reserve associated with cognitive performance and hippocampal volume. Brain: a journal of neurology, 143(2), 622–634. https://doi.org/10.1093/brain/awz383.

Peters, R., Xu, Y., Fitzgerald, O., Aung, H. L., Beckett, N., Bulpitt, C., Chalmers, J., Forette, F., Gong, J., Harris, K., Humburg, P., Matthews, F. E., Staessen, J. A., Thijs, L., Tzourio, C., Warwick, J., Woodward, M., Anderson, C. S., & Dementia rIsk REduCTion (DIRECT) collaboration. (2022). Blood pressure lowering and prevention of dementia: an individual patient data meta-analysis. European Heart Journal, 43(48), 4980–4990.

Pleger, B., Dinse, H. R., Ragert, P., Schwenkreis, P., Malin, J. P., & Tegenthoff, M. (2001). Shifts in cortical representations predict human discrimination improvement. Proceedings of the National Academy of Sciences of the United States of America, 98(21), 12255–12260. https://doi.org/10.1073/pnas.191176298.

Pleger, B., Wilimzig, C., Nicolas, V., Kalisch, T., Ragert, P., Tegenthoff, M., & Dinse, H. R. (2016). A complementary role of intracortical inhibition in age-related tactile degradation and its remodelling in humans. Scientific reports, 6, 27388. https://doi.org/10.1038/srep27388.

Pohlack, S. T., Meyer, P., Cacciaglia, R., Liebscher, C., Ridder, S., & Flor, H. (2014). Bigger is better! Hippocampal volume and declarative memory performance in healthy young men. Brain structure & function, 219(1), 255–267. https://doi.org/10.1007/s00429-012-0497-z.

Ragert, P., Schmidt, A., Altenmüller, E., & Dinse, H. R. (2004). Superior tactile performance and learning in professional pianists: evidence for meta-plasticity in musicians. In European Journal of Neuroscience, 19 (2), 473–478. https://doi.org/10.1111/j.0953-816x.2003.03142.x.

Schreiber, S., Bernal, J., Arndt, P., Schreiber, F., Müller, P., Morton, L., Braun-Dullaeus, R. C., Valdés-Hernández, M. D. C., Duarte, R., Wardlaw, J. M., Meuth, S. G., Mietzner, G.,

Vielhaber, S., Dunay, I. R., Dityatev, A., Jandke, S., & Mattern, H. (2023). Brain Vascular Health in ALS Is Mediated through Motor Cortex Microvascular Integrity. Cells , 12(6). https://doi.org/10.3390/cells12060957.

Schwenkreis, P., El Tom, S., Ragert, P., Pleger, B., Tegenthoff, M., & Dinse, H. R. (2007). Assessment of sensorimotor cortical representation asymmetries and motor skills in violin players. The European Journal of Neuroscience, 26(11), 3291–3302.

Seiler, A., Schöngrundner, S., Stock, B., Nöth, U., Hattingen, E., Steinmetz, H., Klein, J. C., Baudrexel, S., Wagner, M., Deichmann, R., & Gracien, R. M. (2020). Cortical aging - new insights with multiparametric quantitative MRI. *Aging*, *12*(16), 16195–16210. https://doi.org/10.18632/aging.103629.

Sethian, J. A. (1999). Level Set Methods and Fast Marching Methods: Evolving Interfaces in Computational Geometry, Fluid Mechanics, Computer Vision, and Materials Science. Cambridge University Press.

Stüber, C., Morawski, M., Schäfer, A., Labadie, C., Wähnert, M., Leuze, C., Streicher, M., Barapatre, N., Reimann, K., Geyer, S., Spemann, D., & Turner, R. (2014). Myelin and iron concentration in the human brain: a quantitative study of MRI contrast. NeuroImage, 93 Pt 1, 95–106. https://doi.org/10.1016/j.neuroimage.2014.02.026.

Sui, Y. V., Masurkar, A. V., Rusinek, H., Reisberg, B., & Lazar, M. (2022). Cortical myelin profile variations in healthy aging brain: A T1w/T2w ratio study. NeuroImage, 264, 119743. https://doi.org/10.1016/j.neuroimage.2022.119743.

Sullivan, L. M., Weinberg, J., & Keaney, J. F., Jr. (2016). Common Statistical Pitfalls in Basic Science Research. Journal of the American Heart Association, 5(10). https://doi.org/10.1161/JAHA.116.004142.

Tardif, C. L., Schäfer, A., Waehnert, M., Dinse, J., Turner, R., Bazin, P.-L. (2015). Multi-contrast multi-scale surface registration for improved alignment of cortical areas. NeuroImage, 111, 107–122. doi:10.1016/j.neuroimage.2015.02.005.

Thornbury, J. M., & Mistretta, C. M. (1981). Tactile sensitivity as a function of age. Journal of gerontology, 36(1), 34–39. https://doi.org/10.1093/geronj/36.1.34.

Tsushima, Y., Aoki, J., & Endo, K. (2003). Brain microhemorrhages detected on T2*-weighted gradient-echo MR images. AJNR. American journal of neuroradiology, 24(1), 88–96.

Ungvari, Z., Toth, P., Tarantini, S., Prodan, C. I., Sorond, F., Merkely, B., & Csiszar, A. (2021). Hypertension-induced cognitive impairment: from pathophysiology to public health. Nature Reviews. Nephrology, 17(10), 639–654.

Vieluf, S., Godde, B., Reuter, E. M., & Voelcker-Rehage, C. (2013). Age-related differences in finger force control are characterized by reduced force production. Experimental brain research, 224(1), 107–117. https://doi.org/10.1007/s00221-012-3292-4.

Vockert, N., Perosa, V., Ziegler, G., Schreiber, F., Priester, A., Spallazzi, M., Garcia-Garcia, B., Aruci, M., Mattern, H., Haghikia, A., Düzel, E., Schreiber, S., Maass, A. (2021). Hippocampal vascularization patterns exert local and distant effects on brain structure but not vascular pathology in old age. Brain communications, 3(3), fcab127. https://doi.org/10.1093/braincomms/fcab127.

Voelcker-Rehage, C., & Alberts, J. L. (2005). Age-related changes in grasping force modulation. Experimental brain research, 166(1), 61–70. https://doi.org/10.1007/s00221-005-2342-6

Waehnert, M., Dinse, J., Weiss, M., Streicher, M., Waehnert, P., Geyer, S., Bazin, P.-L. (2014). Anatomically motivated modelling of cortical laminae. NeuroImage, 93, 210–220. doi:10.1016/j.neuroimage.2013.03.078.

Wardlaw, J. M., Smith, E. E., Biessels, G. J., Cordonnier, C., Fazekas, F., Frayne, R., Lindley, R. I., O'Brien, J. T., Barkhof, F., Benavente, O. R., Black, S. E., Brayne, C., Breteler, M., Chabriat, H., Decarli, C., de Leeuw, F. E., Doubal, F., Duering, M., Fox, N. C., Greenberg, S., … STandards for ReportIng Vascular changes on nEuroimaging (STRIVE v1) (2013). Neuroimaging standards for research into small vessel disease and its contribution to ageing and neurodegeneration. The Lancet. Neurology, 12(8), 822–838. https://doi.org/10.1016/S1474-4422(13)70124-8.

Yousry, T. A., Schmid, U. D., Alkadhi, H., Schmidt, D., Peraud, A., Buettner, A., & Winkler, P. (1997). Localization of the motor hand area to a knob on the precentral gyrus. A new

landmark. Brain : a journal of neurology, 120 (Pt 1), 141–157. https://doi.org/10.1093/brain/120.1.141.

Yushkevich, P. A., Piven, J., Hazlett, H. C., Smith, R. G., Ho, S., Gee, J. C., Gerig, G. (2006). User-guided 3D active contour segmentation of anatomical structures: significantly improved efficiency and reliability. NeuroImage, 31(3), 1116–1128. https://doi.org/10.1016/j.neuroimage.2006.01.015.

Supplementary Material

Supplementary Methods

Tactile detection task

Tactile detection thresholds of the right index fingertip were assessed using fine hair stimuli (Semmes-Weinstein monofilaments; Baseline, Fabrication Enterprises Inc., White Plains, NY, USA; stimuli intensities: 0.008 g, 0.02 g, 0.04 g, 0.07 g, 0.16 g, 0.4 g, 0.6 g, 1.0 g, 1.4 g, 2.0 g). Stimuli were manually applied to a predefined skin area (circle with 2mm diameter) at an angle of approximately 90 degree, for one second (Mücke et al. 2014). Stimulus application was guided by auditory cues (Psychophysics Toolbox for MATLAB R2017b; Brainard et al. 1997). All participants sat in front of a screen that signalled the beginning and ending of stimulus intervals and listened to white noise via headphones. The right hand (palm facing upwards) was fixated on a pillow behind a paper wall, preventing participants from seeing their own hand and the experimenter. In a two-alternative forced choice paradigm, participants chose one of two possible time intervals that contained the stimulation (randomly applied in the first or second interval) (Gescheider et al. 1996; Thornbury & Mistretta 1981). Application of tactile monofilaments followed a 3-down/1-up staircase with two interleaved staircases, one starting at a 0.02 gram and the other starting at 0.4 gram. The stimulus weight was increased by one step after each error, and decreased by one step after every three correct responses, until stable performance was reached (Gescheider et al. 1996). The experiment was finished when for the last 30 trials the standard variation in stimulus intensity was 1 step or less (Gescheider et al. 1996), or when the maximum number of 100 trials was reached. The participant‘s tactile detection threshold was defined as the mean stimulus intensity across reversal points (change of response from correct to incorrect or incorrect to correct) within the period of stable performance (i.e., the last 10 trials) (Thornbury & Mistretta 1981). The experiment took approximately 12 min. Stimulus intensities were transformed logarithmically on a 1/10th milligram scale (log 10 0.1mg). Lower values indicate higher tactile sensitivity to mechanical forces.

Two-point discrimination task

We also assessed tactile 2-point discrimination performance of the right index fingertip (similar to Kalisch et al., 2008; Kuehn et al., 2017; Pleger et al., 2016). Stimulation was applied by two

rounded pins (diameter=0.4 mm) simultaneously touching the skin. A custom-made, fully automatic stimulation device moved the pins up and down (controlled by Presentation version 16.5, Neurobehavioral Systems, Inc., Albany, CA, USA). The amplitude of pin movement was adjusted to the individual detection threshold, but was at least set to 1.2 mm. Spacing between pins ranged from 0.7 to 2.8 mm (in steps of 0.3 mm) for younger adults and from 0.7 to 6.3 mm (in steps of 0.8 mm) for older adults. A single pin was included as control condition. Pin spacing was vertically adjusted by a rotating disc containing all possible conditions (n=9). In a two-alternative forced-choice paradigm, pin conditions were pseudo-randomly presented. Participants indicated whether they perceived one or two single pins touching their fingertip. They were instructed to give the answer 'two pins felt' only if they were certain. The hand was covered by a white box during the task. Each run included 90 trials (10 repetitions per pin condition). Unique sequences of pin spacing conditions were used per participant and run. All participants completed two runs. Intertrial intervals were pseudo-randomized and varied between 1 to 5 seconds. 2PD thresholds were calculated based on the second run. Answers "two pins felt" were fitted as percentages across ascending pin distances. A binary logistic regression was used to fit the data (glmfit function, Statistics Toolbox for MATLAB R2017b). The 2PD threshold was taken from the pin distance where the 50 percent level crossed the fitted sigmoid curve (e.g. Kalisch et al., 2008; Kalisch et al., 2009; Kuehn et al., 2017; Pleger et al., 2001). Lower values indicate higher spatial acuity.

Sensorimotor integration

Sensorimotor integration was assessed with a custom made pressure sensor (held between the thumb and index finger of the right hand) (Vieluf et al., 2013). Reference forces that were to be matched ranged from 5% to 25% of the individual maximum grip force to avoid muscle fatigue (Voelcker-Rehage & Alberts, 2005). Participants solved a visuo-motor matching task, demanding them to continuously adjust the grip force (Gryga et al., 2012, Vieluf et al., 2013). Applied forces were sampled at a frequency of 100 Hz and projected on screen at a refresh rate of 60 Hz. The task was controlled by the software package Presentation (version 16.5, Neurobehavioral Systems, Inc., Albany, CA, USA). Each trial contained a unique pseudo-randomized sequence of 10 position changes at five different amplitudes (5%, 10%, 15%, 20%, 25% of maximum grip force), leading to a mean frequency of 0.25 Hz. After a period of task familiarisation (Gryga et al., 2012, Voelcker-Rehage & Alberts, 2005), all participants performed the task for a total

duration of 20 seconds. One run contained 15 trials with intertrial intervals of 10 seconds, lasting about 8 minutes in total. All participants performed two runs that were separated by a 5-minute resting period. After each trial, participants received feedback about their individual performance level on screen. We monitored the time (in seconds) the controllable bar was within a given percentage above (2.5%) and below (2.5%) the target line (upper edge of the reference bar) (Vieluf et al., 2013; Voelcker-Rehage & Alberts, 2005). Higher values reflect better sensorimotor integration.

Supplementary Tables and Figures

	Younger Adults			Older Adults		
Task	Mean ± SD	Value Range	# Extreme Outliers	Mean ± SD	Value Range	# Extreme Outliers
Tactile Detection	0.30 ± 0.08	0.22 - 0.44	0	0.27 ± 0.04	0.21 - 0.34	0
Tactile 2-Point Discrimination	0.53 ± 0.16	0.41 - 0.79	0	0.33 ± 0.07	0.19 - 0.51	0
Sensorimotor Integration	8.24 ± 2.56	4.83 - 12.11	0	5.78 ± 1.20	3.45 - 7.37	0

Supplementary Table 1. Sensorimotor performance of younger and older adults. Tactile detection (given in 1/[log10 0.1 mg]) and tactile two-point discrimination (given in 1/mm) were tested at the right index finger. Sensorimotor integration (given as precision grip accuracy in seconds) involved the thumb and the index finger. To ensure that higher values indicate better performance, tactile detection thresholds and tactile 2-point discrimination thresholds were reversed. Extreme outliers are defined as data points smaller or greater than the mean ± 3 standard deviations (SD).

Effect	Conditions	Mean (ms)	SEM (ms)	Statistics DFn	DFd	F	p	η_G^2
Age	Young	1710.74	15.66	1	33	0.137	0.713	0.003
	Old	1702.41	16.12					
Brain Area	M1	1680.95	12.30	1	33	41.597	2.585×10^{-7}	0.086
	S1	1732.19	11.52					
Cortical depth	Deep	1511.72	12.38	3	31	1148.357	4.760×10^{-43}	0.743
	Inner Middle	1649.06	11.22					
	Outer Middle	1770.39	10.10					
	Superficial	1895.13	13.94					
Distance	2.01 - 4 mm	1719.03	12.16	3	31	6.494	0.009	0.014
	4.01 - 6 mm	1712.38	11.53					
	6.01 - 8 mm	1701.47	10.89					
	8.01 - 10 mm	1693.41	12.87					
Age x Distance	Young / 2.01 - 4 mm	1740.50	16.95	3	31	19.232	1.447×10^{-5}	0.040
	Young / 4.01 - 6 mm	1728.96	16.06					
	Young / 6.01 - 8 mm	1702.08	15.18					
	Young / 8.01 - 10 mm	1671.42	17.94					
	Old / 2.01 - 4 mm	1697.57	17.44					
	Old / 4.01 - 6 mm	1695.80	16.53					
	Old / 6.01 - 8 mm	1700.87	15.62					
	Old / 8.01 - 10 mm	1715.39	18.46					
Age x Brain Area	Young / M1	1697.34	17.15	1	33	2.116	0.155	0.005
	Old / M1	1682.57	17.64					
	Young / S1	1742.14	16.06					
	Old / S1	1722.25	16.53					
Brain Area x Distance	M1 / 2.01 - 4 mm	1704.16	12.67	3	31	5.407	0.015	0.007
	M1 / 4.01 - 6 mm	1687.94	11.69					
	M1 / 6.01 - 8 mm	1671.56	11.81					
	M1 / 8.01 - 10 mm	1660.16	16.50					
	S1 / 2.01 - 4 mm	1733.91	12.96					
	S1 / 4.01 - 6 mm	1736.82	12.58					
	S1 / 6.01 - 8 mm	1731.39	11.47					
	S1 / 8.01 - 10 mm	1726.65	12.68					
Age x Brain Area x Distance	Young / M1 / 2.01 - 4 mm	1725.63	17.66	3	31	3.714	0.024	0.005
	Young / M1 / 4.01 - 6 mm	1702.89	16.30					
	Young / M1 / 6.01 - 8 mm	1666.23	16.46					
	Young / M1 / 8.01 - 10 mm	1622.62	23.00					
	Young / S1 / 2.01 - 4 mm	1755.36	18.06					
	Young / S1 / 4.01 - 6 mm	1755.03	17.53					
	Young / S1 / 6.01 - 8 mm	1737.92	15.99					
	Young / S1 / 8.01 - 10 mm	1720.23	17.68					
	Old / M1 / 2.01 - 4 mm	1682.68	18.18					
	Old / M1 / 4.01 - 6 mm	1672.99	16.77					
	Old / M1 / 6.01 - 8 mm	1676.88	16.94					
	Old / M1 / 8.01 - 10 mm	1697.71	23.66					
	Old / S1 / 2.01 - 4 mm	1712.45	18.58					
	Old / S1 / 4.01 - 6 mm	1718.60	18.04					
	Old / S1 / 6.01 - 8 mm	1724.86	16.45					
	Old / S1 / 8.01 - 10 mm	1733.07	18.19					

Supplementary Table 2. ANOVA Results for qT1 values. Results for the ANOVA on qT1 values with factors age (younger, older), cortical depth (SF, OM, IM, DP), brain area (S1, M1) and venous distance (4 distances, excluding the distance 0.01 - 2 mm). Given are mean qT1 values in milliseconds (Mean), degrees of freedom of the numerator (DFn), degrees of freedom of the denominator (DFd), p-values (p), and effect sizes (nG^2). P-values below 0.05 are considered as significant.

Effect	Conditions	Mean (ppm)	SEM (ppm)	Statistics				
				DFn	DFd	F	p	η_G^2
Age	Young	0.0123	0.00048	1	33	39.885	3.824×10^{-7}	0.337
	Old	0.0167	0.00050					
Brain Area	M1	0.0160	0.00042	1	33	78.835	2.912×10^{-10}	0.189
	S1	0.0130	0.00035					
Cortical depth	Deep	0.0115	0.00028	3	31	134.910	1.173×10^{-19}	0.264
	Inner Middle	0.0144	0.00038					
	Outer Middle	0.0162	0.00045					
	Superficial	0.0158	0.00040					
Distance	2.01 - 4 mm	0.0140	0.00037	3	31	10.687	4.384×10^{-4}	0.050
	4.01 - 6 mm	0.0137	0.00029					
	6.01 - 8 mm	0.0147	0.00036					
	8.01 - 10 mm	0.0155	0.00057					
Age x Distance	Young / 2.01 - 4 mm	0.0118	0.00051	3	31	0.052	0.911	2.525×10^{-4}
	Young / 4.01 - 6 mm	0.0115	0.00040					
	Young / 6.01 - 8 mm	0.0125	0.00050					
	Young / 8.01 - 10 mm	0.0134	0.00079					
	Old / 2.01 - 4 mm	0.0163	0.00052					
	Old / 4.01 - 6 mm	0.0159	0.00042					
	Old / 6.01 - 8 mm	0.0169	0.00051					
	Old / 8.01 - 10 mm	0.0177	0.00082					
Age x Brain Area	Young / M1	0.0128	0.00058	1	33	38.484	5.306×10^{-7}	0.102
	Old / M1	0.0192	0.00060					
	Young / S1	0.0119	0.00049					
	Old / S1	0.0142	0.00051					
Brain Area x Distance	M1 / 2.01 - 4 mm	0.0156	0.00042	3	31	0.695	0.485	0.002
	M1 / 4.01 - 6 mm	0.0152	0.00032					
	M1 / 6.01 - 8 mm	0.0163	0.00050					
	M1 / 8.01 - 10 mm	0.0168	0.00072					
	S1 / 2.01 - 4 mm	0.0124	0.00038					
	S1 / 4.01 - 6 mm	0.0122	0.00035					
	S1 / 6.01 - 8 mm	0.0132	0.00037					
	S1 / 8.01 - 10 mm	0.0143	0.00053					
Age x Brain Area x Distance	Young / M1 / 2.01 - 4 mm	0.0129	0.00059	3	31	8.767	0.001	0.020
	Young / M1 / 4.01 - 6 mm	0.0122	0.00045					
	Young / M1 / 6.01 - 8 mm	0.0127	0.00070					
	Young / M1 / 8.01 - 10 mm	0.0132	0.00101					
	Young / S1 / 2.01 - 4 mm	0.0107	0.00052					
	Young / S1 / 4.01 - 6 mm	0.0107	0.00049					
	Young / S1 / 6.01 - 8 mm	0.0124	0.00051					
	Young / S1 / 8.01 - 10 mm	0.0137	0.00074					
	Old / M1 / 2.01 - 4 mm	0.0183	0.00061					
	Old / M1 / 4.01 - 6 mm	0.0182	0.00046					
	Old / M1 / 6.01 - 8 mm	0.0199	0.00072					
	Old / M1 / 8.01 - 10 mm	0.0205	0.00104					
	Old / S1 / 2.01 - 4 mm	0.0142	0.00054					
	Old / S1 / 4.01 - 6 mm	0.0137	0.00051					
	Old / S1 / 6.01 - 8 mm	0.0140	0.00053					
	Old / S1 / 8.01 - 10 mm	0.0148	0.00077					

Supplementary Table 3. ANOVA Results for pQSM values. Results for the ANOVA on pQSM values with factors age (younger, older), cortical depth (SF, OM, IM, DP), brain area (S1, M1) and venous distance (4 distances, excluding the distance 0.01 - 2 mm). Given are mean qT1 values in milliseconds (Mean), degrees of freedom of the numerator (DFn), degrees of freedom of the denominator (DFd), p-values (p), and effect sizes (nG^2). P-values below 0.05 are considered as significant.

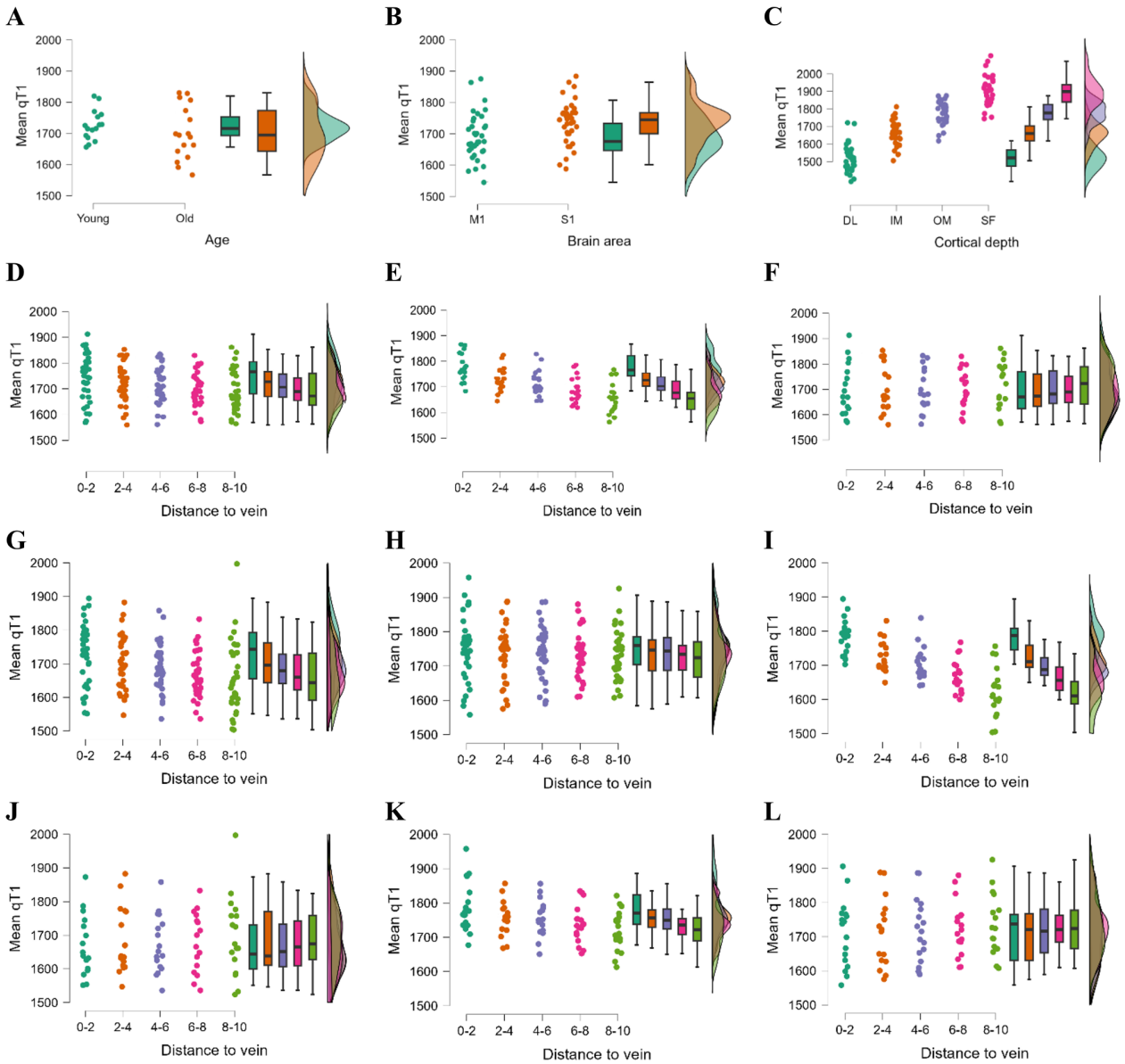

Supplementary Figure 1. Raincloud plots of mean qT1 values for tested ANOVA conditions. A: Younger and older adults **B:** M1 and S1, **C:** Cortical depths **D:** Distance to the nearest vein **E:** Distance to the nearest vein for younger adults **F:** Distance to the nearest vein for older adults **G:** Distance to the nearest vein for M1 **H:** Distance to the nearest vein for S1 **I:** Distance to the nearest vein for younger adults in M1 **J:** Distance to the nearest vein for older adults in M1 **K:** Distance to the nearest vein for younger adults in S1 **L:** Distance to the nearest vein for older adults in S1. DL = deep layer, IM = inner middle layer, OM = outer middle layer, SF = superficial layer. For brain area: M1 = primary motor cortex, S1 = somatosensory cortex.

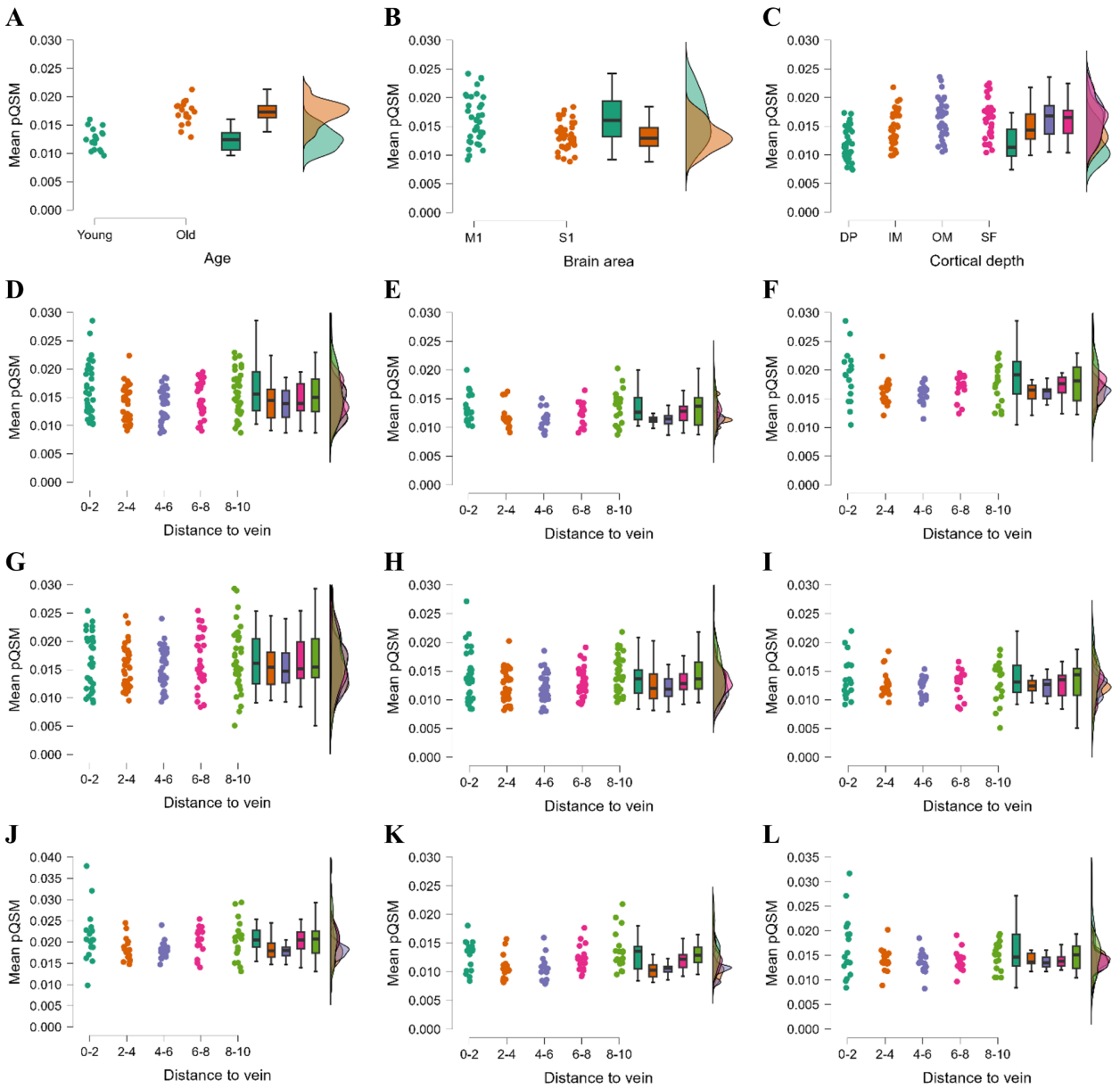

Supplementary Figure 2. Raincloud plots of mean pQSM values for tested ANOVA conditions. A: Younger and older adults **B:** M1 and S1 **C:** Cortical depths **D:** Distance to the nearest vein **E:** Distance to the nearest vein for younger adults **F:** Distance to the nearest vein for older adults **G:** Distance to the nearest vein for M1 **H:** Distance to the nearest vein for S1 **I:** Distance to the nearest vein for younger adults in M1 **J:** Distance to the nearest vein for older adults in M1 **K:** Distance to the nearest vein for younger adults in S1 **L:** Distance to the nearest vein for older adults in S1. DL = deep layer, IM = inner middle layer, OM = outer middle layer, SF = superficial layer. For brain area: M1 = primary motor cortex, S1 = somatosensory cortex.